



HAL
open science

Bridging the spatial gaps of the Ammonia Monitoring Network using satellite ammonia measurements

Rui Wang, Da Pan, Xuehui Guo, Sun Kang, Lieven Clarisse, Martin van Damme, Pierre-François Coheur, Cathy Clerbaux, Melissa Puchalski, Mark A Zondlo

► **To cite this version:**

Rui Wang, Da Pan, Xuehui Guo, Sun Kang, Lieven Clarisse, et al.. Bridging the spatial gaps of the Ammonia Monitoring Network using satellite ammonia measurements. Atmospheric Chemistry and Physics Discussions, In press, 10.5194/egusphere-2023-190 . insu-04030753v1

HAL Id: insu-04030753

<https://insu.hal.science/insu-04030753v1>

Submitted on 15 Mar 2023 (v1), last revised 19 Oct 2023 (v2)

HAL is a multi-disciplinary open access archive for the deposit and dissemination of scientific research documents, whether they are published or not. The documents may come from teaching and research institutions in France or abroad, or from public or private research centers.

L'archive ouverte pluridisciplinaire **HAL**, est destinée au dépôt et à la diffusion de documents scientifiques de niveau recherche, publiés ou non, émanant des établissements d'enseignement et de recherche français ou étrangers, des laboratoires publics ou privés.



Distributed under a Creative Commons Attribution 4.0 International License



Bridging the spatial gaps of the Ammonia Monitoring Network using satellite ammonia measurements

Rui Wang¹, Da Pan¹, Xuehui Guo¹, Kang Sun^{2,3}, Lieven Clarisse⁴, Martin Van Damme^{4,5}, Pierre-François Coheur⁴, Cathy Clerbaux^{4,5,6}, Melissa Puchalski⁷, and Mark A. Zondlo^{1*}

5 ¹Department of Civil and Environmental Engineering, Princeton University, Princeton, NJ, USA

²Department of Civil, Structural and Environmental Engineering, University at Buffalo, Buffalo, NY, USA

³Research and Education in eNergy, Environment and Water (RENEW) Institute, University at Buffalo, Buffalo, NY, USA

⁴Université libre de Bruxelles (ULB), Spectroscopy, Quantum Chemistry and Atmospheric Remote Sensing (SQUARES), Brussels, Belgium

10 ⁵Royal Belgian Institute for Space Aeronomy, Brussels, Belgium

⁶LATMOS/IPSL, Sorbonne Université, UVSQ, CNRS, Paris, France

⁷Office of Air and Radiation, US Environmental Protection Agency, Washington, DC, USA

15 *Correspondence to:* Mark A. Zondlo (mzondlo@princeton.edu)

Abstract. Ammonia (NH₃) is a key precursor to fine particulate matter (PM_{2.5}) and a primary form of reactive nitrogen. The limited observations of NH₃ hinders further understanding of its impacts on air quality, climate, and biodiversity. Currently, NH₃ ground monitoring networks are limited in number across the globe, and even in the most established networks, large spatial gaps exist between sites and only a few sites have records that span longer than a decade. Satellite NH₃ observations can be used to discern trends and fill spatial gaps in networks, but many factors influence the syntheses of the vastly different spatiotemporal scales between surface network and satellite measurements. To this end, we intercompared surface NH₃ data from the Ammonia Monitoring Network (AMoN) and satellite NH₃ total columns from the Infrared Atmospheric Sounding Interferometer (IASI) in the contiguous United States (CONUS) and then performed trend analyses using both datasets. We explored the sensitivity of correlations between the two datasets to factors such as satellite data availability and distribution over the surface measurement period as well as agreement within selected spatial and temporal windows. Given the short lifetime of atmospheric ammonia and consequently sharp gradients, smaller spatial windows show better agreement than larger ones except in areas of relatively uniform, low concentrations where large windows and more satellite measurements improve the signal-to-noise ratio. A critical factor in the comparison is having satellite measurements across most of the measurement period of the monitoring site. When IASI data are available for at least 80% days of AMoN's 2-week sampling period within a 25 km spatial window of a given site, IASI NH₃ column concentrations and the AMoN NH₃ surface concentrations have a correlation of 0.74, demonstrating the feasibility of using satellite NH₃ columns to bridge the spatial gaps existing in the surface network NH₃ concentrations. Both IASI and AMoN show increasing NH₃ concentrations across CONUS (median: 6.8%·yr⁻¹ vs. 6.7%·yr⁻¹) in the last decade (2008 - 2018), stressing the rising importance of NH₃ in terms of nitrogen deposition. NH₃



35 trends for AMoN sites correlates with IASI NH₃ trend IASI and AMoN NH₃ trend ($r = 0.66$) and show a similar spatial pattern,
with the highest increases in the Midwest and eastern U.S., and NH₃ trend for AMoN sites correlates with IASI NH₃ trend (r
= 0.66). In spring and summer, increases of NH₃ were larger than 10%·yr⁻¹ in the eastern U.S. and Midwest (cropland
dominated) and western U.S. (pastureland dominated), respectively. In terms of trend in NH₃ hotpots (defined as regions where
the IASI NH₃ column is larger than the 95th percentile of 11-year CONUS map, 6.7×10^{15} molec/cm²), these largest emissions
40 sources are also experiencing increasing concentrations over time with the median of NH₃ trend is 4.7% · yr⁻¹. IASI data show
large NH₃ increases in urban areas (8.1%·yr⁻¹), including 8 of the top 10 most populous regions in the CONUS, where AMoN
sites are sparse. The increasing NH₃ could have detrimental effects on nearby eco-sensitive regions through nitrogen deposition
and on aerosol chemistry in the densely populated urban areas, hence needs immediate attention.

45 1 Introduction

Gas phase ammonia (NH₃) is the most abundant alkaline gas in the atmosphere, mainly emitted from agricultural activities
such as nitrogen fertilizer applications and livestock waste volatilization (Bouwman et al., 1997; Paulot et al., 2014). As a
major precursor to fine particulate matter (PM_{2.5}), NH₃ critically affects aerosol heterogeneous chemistry, air quality, visibility,
human health, and climate (Hauglustaine et al., 2014; Hill et al., 2019; Lawal et al., 2018; Malm et al., 2004). Ammonia
50 neutralizes sulfuric acid (H₂SO₄) and nitric acid (HNO₃) in the atmosphere to form ammoniated aerosols, ammonium sulfate
(NH₄)₂SO₄) and ammonium nitrate (NH₄NO₃), which in total can contribute to more than 50 % of total PM_{2.5} mass (Feng et
al., 2020). NH₄NO₃ is critical during wintertime haze periods because the cold and humid condition favor its formation (Shah
et al., 2018; Zhai et al., 2021). Besides, NH₃ plays an important role in the nitrogen cycle. Wet deposition of NH₄⁺ dominates
the wet inorganic nitrogen deposition at nearly 70% of monitoring sites in the United States (Li et al., 2016). Total NH_x
55 (≡NH₃(g) + NH₄⁺(aq)) deposition is expected to become even more dominant in the future because NO_x emissions decrease
under pollution control while NH₃ emissions are predicted to continue to increase with the rising global food demands (Erisman
et al., 2008; Goldberg et al., 2021; Pinder et al., 2008). Excessive NH₃ deposition in the non-agricultural ecosystems can reduce
biodiversity, result in soil acidification, and increase eutrophication, especially in the sensitive ecosystems (Ellis et al., 2013;
Phoenix et al., 2006).

60 Although NH₃'s importance has been well recognized, routine NH₃ observations are lacking even in countries with
comprehensive monitoring networks, partly due to the difficulty of measuring gas phase NH₃ (von Bobruzki et al., 2010;
Fehsenfeld et al., 2002). The Ammonia Monitoring Network (AMoN) (Puchalski et al., 2015) is the only routine set of NH₃
measurements in the United States, with 110 active AMoN sites in the contiguous United States (CONUS) in 2021, providing
65 high-quality surface observations of NH₃. AMoN data have been used widely for model evaluation and long-term trend
analysis (Butler et al., 2016; Nair et al., 2019; Yao and Zhang, 2016, 2019). AMoN only provides bi-weekly NH₃ observations,



in contrast to monitoring networks for two other important gas phase precursors of $PM_{2.5}$, SO_2 and NO_2 , which provide hourly or daily scale observations. $PM_{2.5}$, SO_2 , and NO_2 are directly regulated as criteria pollutants, however contributions from NH_3 emissions sources must be considered in State Implementation Plan (SIP) demonstrations for areas out of attainment for $PM_{2.5}$, which can be a challenge for areas lacking NH_3 measurements (EPA 2023).

Population weighted $PM_{2.5}$ concentrations are widely used to estimate the health effects of $PM_{2.5}$, however, the sparse number of NH_3 sites with only biweekly or monthly resolution makes it difficult to derive population weighted $PM_{2.5}$ precursor datasets. Gas phase NH_3 is critical to determine the partitioning of the total NH_x (Hennigan et al., 2015), and the lack of gas phase NH_3 observations hampers the evaluation of chemistry models. The ISORROPIA-II thermodynamic model has been extensively adopted to compute the equilibrium composition for the inorganic aerosol systems (Fountoukis and Nenes, 2007) and requires both gas and aerosol phase data as input to provide accurate and robust results (Hennigan et al., 2015). However, the limited number of NH_3 ground monitoring sites currently prevents synthesizing the AMoN NH_3 data with other ground monitoring networks, e.g., IMPROVE, as input for ISORROPIAII (Pan et al., 2020). GEOS-Chem implemented with ISORROPIA-II was found to significantly underestimate gas phase NH_3 and overestimate NH_4^+ in winter (Holt et al., 2015; Nair et al., 2019; Walker et al., 2012), with the normalized NH_4^+ mean biases as high as 86% in January at sites for the Interagency Monitoring of Protected Visual Environments (IMPROVE) (Holt et al., 2015). The lifetime of NH_3 ranges from hours to days, hence large spatiotemporal variability exists (Golston et al., 2020; Miller et al., 2015; Wang et al., 2021), and large spatial gaps exist in the current AMoN. Currently there are no AMoN sites in some states, e.g., North Dakota and South Dakota, and only 12 sites are within the characteristic length scale (12 km) of NH_3 hotspots regions (Wang et al., 2021). Ten national parks in the U.S. are within 100 km of an NH_3 hotspot, and more observations are needed to quantify the impacts of these hotspots on dry NH_3 deposition in these regions (Pan et al., 2021). A lack of long-term AMoN data also hinders the possibility of investigating NH_3 trends in the CONUS. Increasing NH_3 concentrations are observed using AMoN data, yet all of the previous trend analyses are limited to fewer than 20 AMoN sites that may not be representative of NH_3 trends in the CONUS (Butler et al., 2016; Yao and Zhang, 2016, 2019).

Satellite NH_3 observations are on a global and daily basis, providing long-term trends and ubiquitous coverage. Instruments that measure NH_3 include the Infrared Atmospheric Sounding Interferometer (IASI) on the MetOp satellites, Cross-track Infrared Sounder (CrIS) on NOAA and NASA Suomi National Polar-orbiting Partnership (S-NPP), Tropospheric Emission Spectrometer (TES) on NASA Aura satellite, Atmospheric Infrared Sounder (AIRS) on NASA EOS Aqua satellite, and Thermal and Near Infrared Sensor for Carbon Observations – Fourier Transform Spectrometer (TANSO-FTS) on the Greenhouse Gases Observing SATellite (GOSAT) (Clarisse et al., 2009; Shephard et al., 2011; Shephard & Cady-Pereira, 2015; Someya et al., 2020; Warner et al., 2016). Satellite NH_3 data have been widely used to constrain NH_3 emissions, estimate NH_3 deposition, and analyze NH_3 trends (Cao et al., 2020; Chen et al., 2020; Kharol et al., 2018; Van Damme et al., 2021). Van Damme et al. (2021) utilized 11-year IASI NH_3 observations and found a worldwide NH_3 increase (12.8 ± 1.3 %) from



2008 to 2018 with especially large increases in east Asia (75.7 ± 6.3 %) and North America (26.8 ± 4.5 %). Warner et al. (2017) used 14-year AIRS NH_3 measurements and found statistically significant NH_3 increase ($2.61\% \cdot \text{yr}^{-1}$) in the U.S. from 2002 to 2016.

105 The global daily coverage and long-term data record make it possible for satellite observations to fill the spatial and temporal gaps of the current ground monitoring networks. Although limited in numbers, the validations of satellite NH_3 observations with in-situ measurements provide confidence in integrating the two datasets (Guo et al., 2021; Sun et al., 2015). Sun et al. (2015) performed the first daily and pixel scale satellite NH_3 validations using TES NH_3 columns and airborne NH_3 observations in the San Joaquin Valley of California, USA, showing that the differences between the total NH_3 column and the in-situ total column were within 6 %. However, the validation included only 9 TES pixels, and TES is no longer in operation now. Guo et al. (2021) showed that IASI NH_3 columns and NH_3 columns derived from airborne and ground-based NH_3 observations were indistinguishable from one another on daily and pixel bases in Colorado, USA, in summer. All of these validation works were performed in certain seasons and were limited to source regions with high NH_3 concentrations (Guo et al., 2021; Sun et al., 2015; Warner et al., 2016). Ground-based FTIR NH_3 observations provided a better temporal coverage for evaluating IASI and CrIS NH_3 retrievals, however, low concentration sites were excluded from the evaluation and only ~ 10 sites were included across the globe (Dammers et al., 2016; Dammers et al., 2017). Furthermore, FTIR-based measurements also have not been directly validated against in-situ measurements of NH_3 vertical profile themselves.

To capitalize on the benefits of both surface and satellite observations and synthesize these datasets, a detailed understanding of the comparison between IASI NH_3 column concentrations and AMoN NH_3 surface concentrations is necessary. Here we focus on IASI NH_3 measurements because it offers the longest data record (2008 - present) among the satellite NH_3 -measuring instruments. The comparison between AMoN and IASI is complex because AMoN is a ground-based, point measurement integrated over fourteen days, whereas IASI is a space-borne volumetric measurement averaged over the pixel footprint at the instantaneous overpass time. There are several factors that need to be taken into consideration:

125 (1) The extent to which the IASI NH_3 column represents the surface AMoN NH_3 concentration: Knowledge of NH_3 vertical profiles in the atmosphere are limited due to the lack of observational data, and model simulated NH_3 vertical profiles are often biased compared with the airborne measurements (Schiferl et al., 2016). Ammonia is mostly concentrated in the planetary boundary layer (PBL) because of its short lifetime (~hours to days) and surface emission sources (Dentener & Crutzen, 1994; Guo et al., 2021; Sun et al., 2015; Seinfeld & Pandis, 2016). Sun et al. (2015) showed that NH_3 was almost well mixed in the lower PBL, and the TES NH_3 columns were strongly correlated ($R^2 = 0.82$) with the median NH_3 mixing ratios measured at the surface, demonstrating that satellite NH_3 columns could represent the ground NH_3 concentrations. Van Damme et al. (2015) converted IASI NH_3 columns to surface NH_3 concentrations using fixed NH_3 profiles generated by GEOS-Chem, then performed monthly comparisons with ground monitoring networks. IASI derived surface NH_3 observations are in fair



135 agreement with ground observations in Europe, China, and Africa, but are limited to a small number of sites in each region for
a short time range, e.g., 27 sites in Europe in 2011 (Van Damme et al., 2015). Furthermore, the latest IASI NH₃ products have
switched to a new algorithm and no longer use a fixed NH₃ profile (Whitburn et al., 2016; Van Damme et al., 2017).

(2) Optimal spatial window for comparing and integrating satellite pixels and AMoN sites: Previous comparisons of satellite
140 NH₃ retrievals with observations from ground monitoring networks simply averaged the data from the monitoring site within
a coarse model grid (~ 100 km) with the averaged modeling/satellite NH₃ concentration of the whole grid (Kharol et al., 2018;
Nair et al., 2019; Van Damme et al., 2015). If NH₃ concentrations are uniformly distributed within the spatial window,
increasing the spatial window will increase the number of IASI pixels and decrease the signal-to-noise ratio. However, the
spatial heterogeneity of NH₃ is quite large near hotspots due to its short lifetime (Golston et al., 2020; Miller et al., 2015; Wang
145 et al., 2021; Warner et al., 2016). The relationship between spatial window size and satellite/surface measurements agreement
needs to be examined in more details.

(3) Temporal distribution of satellite measurements across the two-week AMoN sampling period: Previous comparisons of
model or satellite products against surface observations did not consider the distribution of IASI measurements during the two-
150 week sampling period (Kharol et al., 2018; Nair et al., 2019; Van Damme et al., 2015). AMoN measures continuously, whereas
a series of cloudy days would preclude any valid satellite measurements. Therefore, any AMoN/satellite comparison is
intrinsically biased towards clear sky days on the satellite side but includes all conditions for the AMoN site.

(4) Number of available IASI pixels in the comparison: Guo et al. (2021) has shown that, even at low column amounts, IASI
155 NH₃ has no known biases. AMoN is an extremely sensitive measurement of NH₃, far more precise than any satellite NH₃
product (NADP, 2023; Van Damme et al., 2017). Therefore, increasing the number of satellite measurements within a certain
spatiotemporal window is expected to improve the signal-to-noise ratio in the satellite measurements and may lead to improved
agreements with AMoN under clean conditions.

160 (5) Regional and seasonal variabilities: Different regional and seasonal patterns are expected to influence the comparison. The
performances of thermal infrared sounders are highly affected by the thermal contrast between the surface air temperature and
skin temperature (Clarisse et al., 2010). In winter, low thermal contrast results in low sensitivity, which explains the low
number of IASI pixels in winter compared to summer (Clarisse et al., 2010; Guo et al., 2021). Kharol et al. (2018) showed that
CrIS surface NH₃ concentrations had an overall mean CrIS–AMoN difference of ~+15%, however, they only averaged CrIS
165 data over the warm season in 2013.

In this study, to demonstrate the capabilities of using IASI NH₃ observations to augment the ground monitoring network, we
performed a comprehensive comparison between IASI and AMoN on weekly/seasonal scales. We directly compare the



170 correlation between IASI NH_3 columns with AMoN surface NH_3 . We avoided direct comparisons when converting column
175 NH_3 into surface concentrations because of possible biases introduced by assuming vertical profiles, boundary layer heights at
local sites, and gas phase - aerosol partitioning. The impacts of the different factors on the comparison are examined in the
context of points raised above. After identifying the most optimal method for comparison, we examined NH_3 trends over
AMoN sites and the larger applicability of using satellite retrievals to discern NH_3 trends over regions and seasons lacking
AMoN data.

175

2 Data and methods

2.1 Satellite NH_3 observations

IASI is an infrared sounder launched on board of the MetOp-A, MetOp-B, and MetOp-C platforms in sun-synchronous orbits
since October 2006, September 2012, and November 2018, respectively. IASI has a swath of 2200 km and provides global
180 coverage twice per day at around 09:30 and 21:30 mean local solar time. At nadir, the IASI footprint has a 12-km diameter.
The first IASI NH_3 product was developed by Clarisse et al. (2009) by converting the brightness temperature differences into
total NH_3 columns. Later on, a flexible and robust retrieval algorithm based on an artificial neural network for IASI (ANNI)
(Whitburn et al., 2016) was developed. The latest version consists of a reanalyzed dataset provided with the European Centre
for Medium-Range Weather Forecasts Re-Analysis v5 (ERA5) as its meteorological input (Van Damme et al., 2017; Van
185 Damme et al., 2021). Because the meteorological input for reanalysis data is coherent in time, it is the more appropriate dataset
to be used to study trends. For the present analyses, we used IASI version 3.1 reanalysis (v3.1r) retrieval product data from the
MetOp/A (2008-2018) and MetOp/B (2013-2018) satellites (limited to cloud fraction $\leq 25\%$). Only the morning orbits were
analyzed because of higher sensitivity than the evening overpasses (Clarisse et al., 2010).

190 2.2 Ground-based observations

AMoN is the only network providing a consistent, long-term record of NH_3 gas concentrations across the United States. AMoN
was established by the National Atmospheric Deposition Program (NADP) in October 2007 and expanded to 19 sites in 2010
and 105 sites in 2018. AMoN deploys Radiello® passive samplers that rely upon diffusion theory, where gas phase NH_3 is
adsorbed onto a cylindrical interior filter and extracted as NH_4^+ to be analyzed by Flow Injection Analysis (FIA). AMoN
195 provides biweekly surface NH_3 concentrations, and the network detection limit is $0.083 \text{ mg NH}_4^+ \text{ L}^{-1}$ ($\sim 0.078 \mu\text{g NH}_3 \text{ m}^{-3}$) for
the 2-week samples in 2020 (NADP, 2023). The Radiello passive samplers were found to be biased low by 37% against
denuders used as reference method (Puchalski et al., 2011). In this study, we are comparing the relative variations instead of
absolute concentrations of IASI and AMoN, therefore the low bias of AMoN measurements is not as relevant to the outcome.



200 We incorporated data from all AMoN sites with one notable exception. Using satellite imagery, we identified that the AMoN
site in Logan, Utah (UT01), is located only ~ 100 m away from a livestock farm. Ammonia concentrations downwind of a
beef/dairy feedlot at this distance are far above background levels and unrepresentative of those at the local-regional scales (1-
10 km) (Golston et al., 2020; Miller et al., 2015; Sun et al., 2018). Concentrations at UT01 are expected to be strongly
dependent upon the extent to which local winds blow directly from that farm to the AMoN site throughout the two-week
205 integration period. Not surprisingly, the UT01 site has the highest annual mean concentration ($16.2 \mu\text{g}/\text{m}^3$) in the entire AMoN
network (three times higher than the next one). Furthermore, this AMoN site may be particularly susceptible to trends in animal
operations or management practices at the farm. While it is possible the measurements of UT01 are representative of the local
region, it is beyond the scope of this work to make such an assessment of its representativeness.

210 2.3 Trend analyses

2.3.1 Oversampled NH_3 maps

From 2008 to 2018, a $0.02^\circ \times 0.02^\circ$ (~ 2 km) annual mean NH_3 map in the CONUS was created each year based on a physical
oversampling algorithm that represents the satellite spatial response functions as generalized 2-D super Gaussian functions
(Sun et al., 2018). This algorithm weighs IASI measurements by their uncertainties which include varying sensitivities to
215 thermal contrast as described in Sun et al. (2018) and Wang et al. (2021). For each year, seasonally averaged oversampling
maps were also generated for spring (March, April, and May, MAM), summer (June, July, and August, JJA), fall (September,
October, and November, SON), and winter (December, January, and February, DJF). For each season, we were able to achieve
sufficiently overlapped IASI pixels through calculating the sum of the unnormalized spatial response function (SRF) of the
oversampling results (Sun et al., 2018; Wang et al., 2021).

220

2.3.2 Mann-Kendall test and Theil-Sen's slope estimator

We use the Mann-Kendall (MK) test and Theil-Sen's slope estimator for NH_3 trend analyses. The non-parametric Mann-
Kendall test and Theil-Sen's slope estimator are widely used in detecting trends of variables in meteorology and hydrology
fields (Ahn and Merwade, 2014; Kendall, 1975; Yue and Wang, 2004). The Kendall rank correlation coefficient, commonly
225 referred to as Kendall's τ coefficient, is a statistic used to measure the rank correlation. An MK test is a non-parametric
hypothesis test for statistical dependence based on the Kendall's τ coefficient. The Theil-Sen's slope estimator is commonly
used to fit a line to data points by calculating the median of the slopes of all lines through pairs of points.

Different from simple linear regression, the Mann-Kendall test and Theil-Sen's slope estimator do not require the data to
230 follow normal distribution and therefore are more robust to any outliers (Yue and Wang, 2004). This method is computationally



efficient and is insensitive to outliers. For skewed and heteroskedastic data, the Theil-Sen estimator can be significantly more accurate than linear least squares regression. For normally distributed data, the Theil-Sen estimator competes well against the least squares in terms of statistical power (Yue and Wang, 2004).

3 IASI & AMoN comparison

235 3.1 Sensitivity to spatial windows

For the initial analysis, we first show the simplest way of comparing the satellite measurements with ground observations. In other words, we center on each AMoN site, average all IASI observations within a given radius of the AMoN site for the sampling time frame (2 weeks) for comparison, and refer to that radius as a spatial window. If the distribution of NH₃ pixels is spatially uniform, increasing the spatial window may improve the correlation between the two because of a larger number of IASI pixels. Larger spatial windows include more IASI pixels than smaller spatial windows but at the expense of potentially not being representative of the AMoN site. In addition, a larger region is likely to encompass NH₃ spatial gradients. In contrast, small spatial windows may only include a limited number of IASI pixels, encompassing more inherent noise in the satellite measurements, especially if close to the detection limit. Each integrated 2-week AMoN measurement for each site was correlated with any relevant satellite data within the spatial window (total of 104 AMoN sites with 16,093 measurements). Correlations between IASI and AMoN for different spatial windows (15 km, 25 km, 50 km, and 100 km) are summarized in Table 1. The minimum spatial window radius of 15 km is based upon an approximate scale for NH₃ hotspots (Wang et al. 2021).

As the spatial window becomes larger, mean temporal coverage (defined as the percentage of days with available IASI data of the 2-week AMoN sampling period) and number of IASI pixels both have significant increases, but the Pearson's r coefficient only increases slightly from 0.35 at a 15 km spatial window to 0.44 at a 100 km spatial window. Indeed, doubling the spatial window from 50 km to 100 km yields an almost tripled mean number of IASI pixels, yet maintains the almost the same correlation with $r = 0.45$ and $r = 0.44$, respectively. This indicates that including IASI pixels at longer distances from the AMoN site may not be representative of the AMoN site, especially near sources or regions with complex topography. The slightly increased r value over spatial window range may result from a tradeoff between averaging spatial gradients versus integrating a larger number of IASI pixels to improve the signal-to-noise ratio of the satellite measurements. To balance these competing effects, we select 25 km as the nominal spatial window for the further comparisons.

260 **Table 1.** AMoN & IASI comparison results for different spatial windows

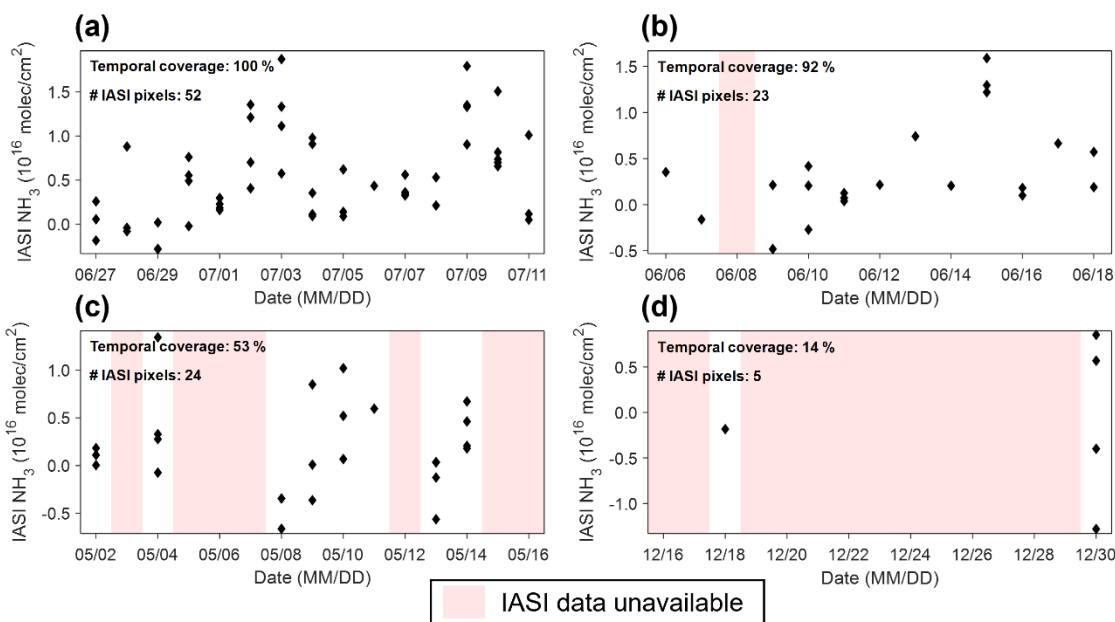
Spatial window	15 km	25 km	50 km	100 km
----------------	-------	-------	-------	--------



Pearson's r	0.35	0.41	0.45	0.44
Mean temporal coverage per pair (%)	31	44	57	71
Mean # IASI pixels per pair	7	17	69	278
# AMoN & IASI pairs	14734	15543	15933	16022

3.2 Sensitivities to temporal coverage and number of IASI pixels

NH₃ is a short-lived species with a complicated diurnal profile (Nair and Yu, 2020) and the potential for large day-to-day concentration changes because of the variability in emissions, wind speed, temperature, PBL height, and aerosol partitioning (Golston et al., 2020; Miller et al., 2015). Thus, the temporal distribution of satellite measurements within the AMoN measurement period may impact the comparison. Fig. 1 illustrates four examples where the number of IASI pixels, and their relative distribution throughout the 2-week AMoN integration period, may impact the comparison (25 km spatial window). An ideal comparison case would have a uniform number of IASI measurements on each day during the approximate 14-day AMoN measurement period, similar to the case shown in Fig. 1a. In this case, there is no specific day having more weight than the other when calculating the biweekly mean. More common, however, are cases where some days have no satellite measurements due to clouds or low thermal contrast. For example, Fig. 1b has one missing day (N=23 satellite measurements) but with an otherwise even distribution throughout the remainder of the period, while Fig. 1c (N=24) has nearly the same number of satellite measurements as Fig. 1b but clustered on only 8 of the 15 days. Finally, there are also many cases where selected day(s) have few or no IASI measurements at all (Fig. 1d). When neither temporal coverage nor the number of IASI pixels are high, one can still calculate the matched IASI NH₃ column for this AMoN sample, but the result is unlikely to be more representative than a more temporally distributed comparison.



280 **Figure 1.** Examples of IASI data temporal coverage over the biweekly AMoN sampling period: (a) several IASI measurements every day during the 2-week sampling period; (b) a few IASI measurements for most time of the 2-week sampling period; (c) many IASI measurements but only in several days during the 2-week sampling period; (d) sparse IASI measurements for only several days during the 2-week sampling period.

285 To this end, we explore the correlation with IASI data's temporal coverage of the 2-week sampling period and total number of IASI pixels within the 2-week AMoN sampling period using the 25 km spatial window. For example, the temporal coverages for Fig. 1 are 100%, 92%, 53%, and 14%, respectively, and the number of IASI pixels are 52, 23, 24, and 5, respectively. The impact of different temporal averaging and number of IASI pixels requirements are summarized in Table 2 and Table 3, respectively. Increasing temporal coverage and number of IASI pixels both yield higher r values than any of the simple spatial windows alone. Table 2 shows that the correlation improves to $r = 0.74$ when the temporal coverage is $\geq 80\%$, suggesting a significant impact of temporal coverage of the IASI data. The IASI and AMoN correlations also increase over a simple spatial window with increasing numbers of IASI pixels, yet the impact is not as strong ($r = 0.63$ for $N \geq 40$) as the sensitivity to temporal coverage.

295

Table 2. The impact of IASI data's temporal coverage for the 2-week AMoN sampling period (25 km spatial window)

IASI temporal coverage per pair (%)	[0, 20)	[20, 50)	[50, 80)	[80, ∞)
-------------------------------------	---------	----------	----------	---------



r	0.17	0.29	0.47	0.74
Mean # IASI pixels per pair	3	13	26	38
# AMoN & IASI pairs	1766	7641	5137	999

Table 3. The impact of # IASI pixels (25 km spatial window)

# IASI pixels per pair	[0, 10)	[10, 20)	[20, 40)	[40, ∞)
r	0.16	0.37	0.50	0.63
Mean temporal coverage per pair (%)	22	42	61	80
# AMoN & IASI pairs	4533	5025	5309	676

300

Because the temporal coverage and number of IASI pixels are not independent variables, additional analyses are conducted to study the sensitivity of these two effects using Monte-Carol method. First, the available dataset is filtered to cases when at least one of the fourteen days have multiple IASI measurements per AMoN measurement, at least 7 days of the 14-day sampling period had at least one IASI measurement, and the total number of IASI pixels is at least 20. The number of days with available IASI measurement is denoted by T. Two opposite approaches are explored for 104 qualified AMoN sites:

305

(1) Maximized temporal coverage (TC_{max}): only one IASI pixel is randomly selected to represent that day, and the total number of IASI pixels equals T ($T \leq 14$). In this case, the temporal coverage is maximized.

310

(2) Minimized temporal coverage (TC_{min}): only days with the largest number of IASI pixels are selected until the total number of IASI pixels equals T ($T \leq 14$). In this case, the temporal coverage is minimized, and the total number of selected IASI pixels is same with TC_{max}.

315

For each AMoN site, we performed the two different sampling strategies for 100 times, then calculated the median r value to represent each site using the maximum and minimum coverage approaches. Fig. 2a shows the histogram and normalized fit of change in r ($\Delta r = TC_{max} - TC_{min}$) for each site between the two scenarios with the number of bins determined by Sturge's



rule. The increased correlation of $\Delta r = 0.45 \pm 0.28$ shows the large impact of temporal coverage. The total number of IASI pixels used for the two strategies were identical.

320 To further investigate the impact of including more IASI pixels after maximizing temporal coverage, we also test the process described in (1) and then randomly added (20-T) more IASI pixels from the remaining IASI pixels and referred to it as TC_max_add. Fig. 2b shows that the changes Δr between TC_max and TC_max_add are small (-0.00 ± 0.05). For the TC_max strategy, the initial number of IASI pixels was between 7 and 14, which means using TC_max_add strategy result in a 43 ~ 186 % increase in the number of IASI pixels compared to TC_max alone. Adding more IASI pixels does not have a significant
325 impact on the r values, indicating that maximized temporal coverage alone is the most important factor when comparing IASI to AMoN stations.

After applying a temporal coverage requirement (temporal coverage ≥ 80 %) to filter the overall dataset, we revisit the sensitivity of the agreement between spatial windows. The smaller spatial window now yields better agreement than the larger
330 spatial windows (Table 4). Compared with Table 1 which has no filter for temporal coverage, the r values in Table 4 increase for all spatial windows. The correlations are clearly better for smaller spatial windows ($r = 0.74$ for 25 km versus $r = 0.48$ for 100 km). In this way, the use of a larger spatial window is indeed a tradeoff between the increasing temporal coverage versus incorporating a larger spatial gradient. The results further demonstrate that the IASI pixels far from the AMoN sites may not be representative to the AMoN site.

335

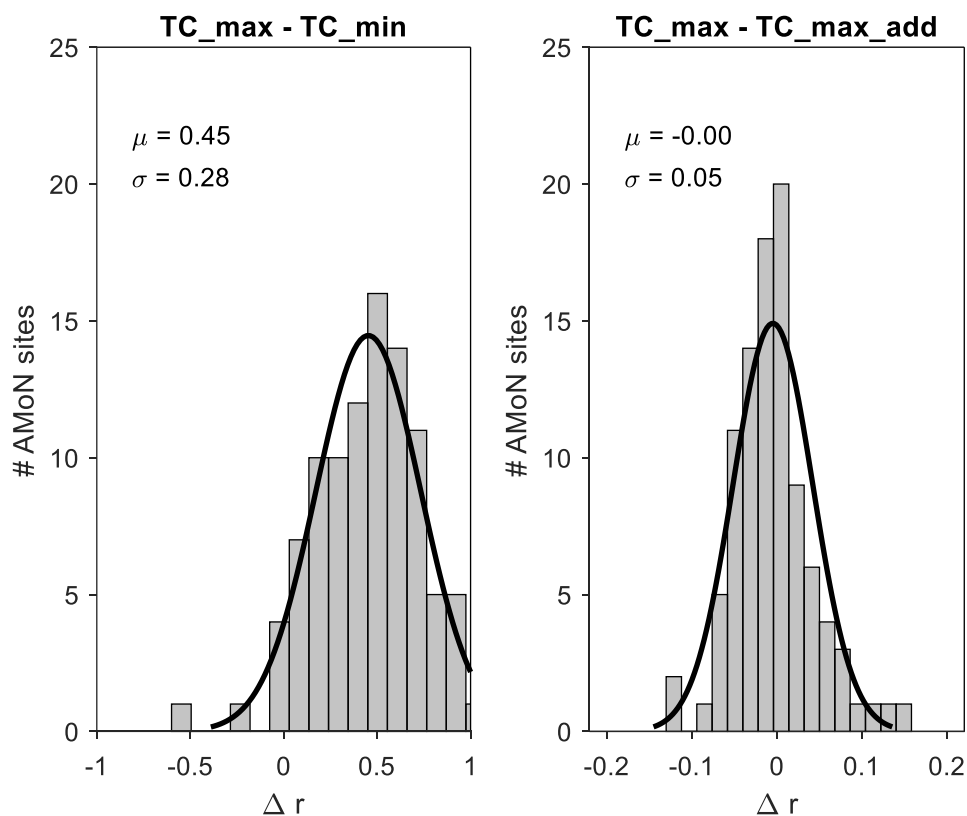


Figure 2. The change in r values for individual AMoN sites using different sampling strategies: **(a)** maximized temporal coverage (TC_max); minimized temporal coverage (TC_min) and **(b)** maximized temporal coverage & randomly adding more pixels (TC_max_add).

Table 4. AMoN & IASI comparison results for different spatial windows (temporal coverage $\geq 80\%$)

Spatial window	15 km	25 km	50 km	100 km
Pearson's r	0.76	0.74	0.58	0.48
Mean # IASI pixels per pair	19	38	119	392
# AMoN & IASI pairs	105	999	3138	6899



3.3 Sensitivity to seasons and temporal averaging

AMoN has similar numbers of measurements in spring (March, April, May), summer (June, July, August), autumn (September, October, November), and winter (December, January, February), while the mean number of IASI pixels (# IASI pixels) per pair in winter is only around half of other seasons (Fig. 3). In winter, low thermal contrasts result in low sensitivity of thermal infrared sounder, which explains the low number of IASI pixels in winter (Clarisse et al., 2010; Guo et al., 2021). The lower sensitivity of the infrared thermal sounder measurements in winter results in higher uncertainties, and thus comparisons between IASI and AMoN are especially important. When temporal coverage is at least 80%, IASI wintertime data still have good agreement with AMoN ($r = 0.61$) although the comparison are limited to only a few AMoN & IASI pairs ($N = 33$). IASI in general only provides a small number of pixels in winter, however, it indeed has the capability of reflecting surface NH_3 variations even in winter.

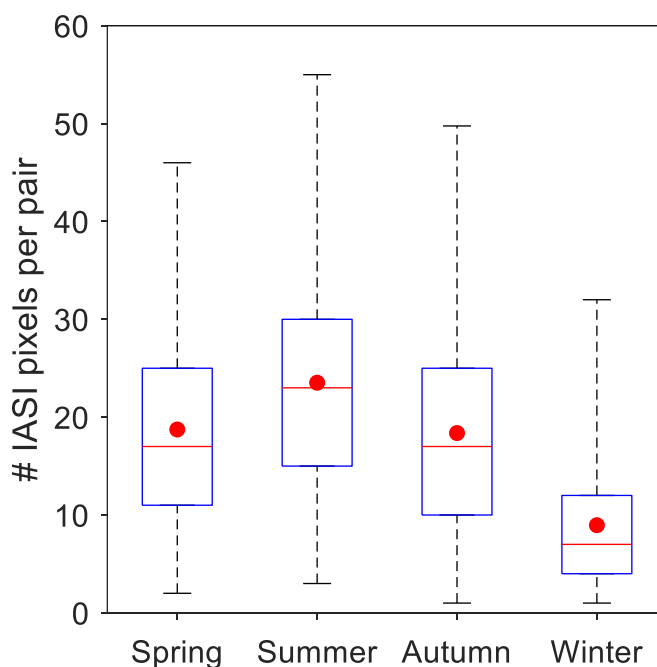


Figure 3. Boxplot of number of IASI pixels per pair for spring, summer, autumn, and winter. The boxes denote the 25th and 75th percentiles, the whiskers denote the 1st and 99th percentiles, and the red dot denotes the mean.

360

The results in 3.1 and 3.2 have already shown the importance of spatial window and temporal coverage. The temporal averaging, such as the tessellation oversampling and physical oversampling, is a common method to achieve a high spatial resolution map by sacrificing the temporal resolution (Sun et al., 2018; Van Damme et al., 2018; Wang et al., 2021). Here we neglect the interannual variability and calculate the multi-year averaged seasonal IASI NH_3 concentrations using the 25 km



365 spatial window. By averaging the multi-year IASI data, the impacts of temporal coverage are alleviated because both temporal
coverages and numbers of IASI pixels increase. Among the 101 AMoN sites with at least one full year data and available IASI
v3.1r NH₃ data, 49 sites show strong agreement with IASI with $r > 0.8$, 29 sites have moderate agreement of $0.5 < r \leq 0.8$,
while 23 sites do not have statistically significant agreements (Fig. 4). If taking all data into consideration, the overall r value
for the CONUS is 0.69. The AMoN sites with higher NH₃ concentrations tend to show better agreements between AMoN and
370 IASI. The median AMoN NH₃ annual mean concentrations for all sites is 0.86 $\mu\text{g}/\text{m}^3$. Most sites with no statistically significant
agreements have a low NH₃ concentration (median: 0.48 $\mu\text{g}/\text{m}^3$). Currently, most AMoN sites are located in low or moderate
NH₃ concentration regions with a lack of sites in the NH₃ hotspots (Wang et al., 2021) and urban areas, complicating the
comparison between AMoN and IASI.

375 The above agreement demonstrates that IASI NH₃ column reflects the variation of the surface NH₃ concentration at seasonal
resolution. For regions without any available ground measurements, IASI NH₃ observations can be used to help better
understand the NH₃ variations. However, large differences exist among the relationships between IASI and AMoN NH₃
concentrations over different AMoN sites (an example of linear regression plot in Fig. 5b). Even for AMoN sites with excellent
correlation ($r > 0.8$), the slopes vary a lot, ranging from $0.08 - 1.4 \times 10^{16}$ molec/cm² per $\mu\text{g}/\text{m}^3$. For instance, two AMoN sites
380 in California, Joshua Tree National Park (CA 67) and Sequoia & Kings Canyon National Park (CA 83), both exhibit great
seasonality agreements with IASI ($r = 0.97$ and $r = 0.99$, respectively) but the slope for CA 83 is 44 % higher than CA 67. The
difference between the slopes suggests that although IASI is able to capture the general seasonality, the relationship between
NH₃ column and surface NH₃ is distinctly different due to complicated topography, meteorology, and other factors at different
AMoN sites.

385

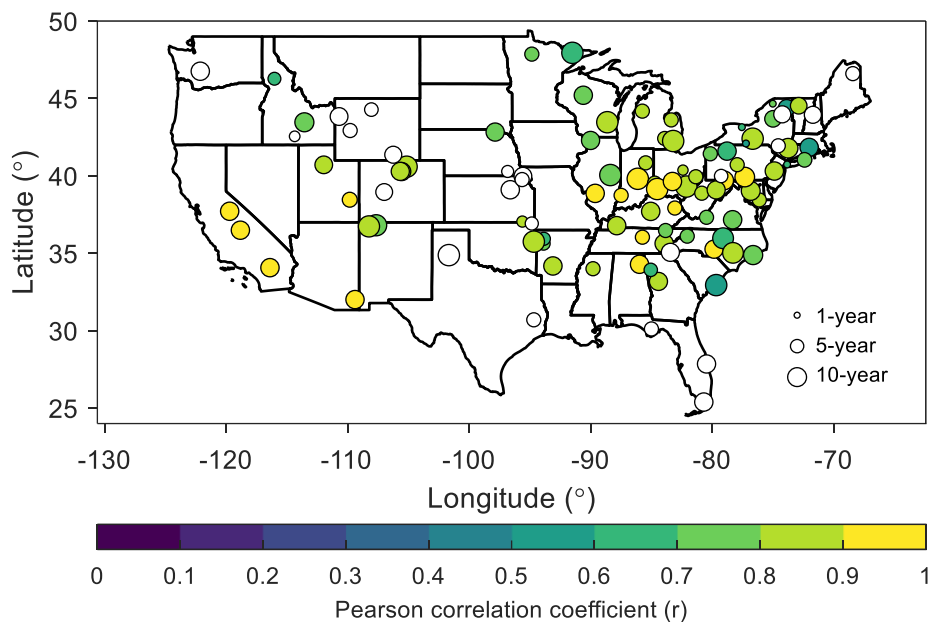


Figure 4. Multi-year averaged comparison results between AMoN sites and the IASI observations within 25 km of the AMoN sites at monthly resolution. Circles without filled color denote the AMoN sites with no statistically significant correlation with IASI. The circle sizes denote the length of AMoN data record.

4 Trend analysis

4.1 Trend in the CONUS

The methodology and comparison results in section 3 demonstrate that IASI NH_3 can be used to estimate regional NH_3 trends over the last decade. In this regard, satellite NH_3 observations will be used to augment the AMoN observed NH_3 trends in the CONUS over the last decade. We include AMoN trend analysis only for sites with full year coverage during 2008 - 2018 (N=13). Strong evidence of increasing NH_3 concentrations in the U.S. comes from both ground-based observations and satellite measurements (Van Damme et al., 2021; Warner et al., 2017; Yao and Zhang, 2016; Yao and Zhang, 2019; Yu et al., 2018). Fig. 5a shows monthly IASI and AMoN timeseries in from Indianapolis, Indiana, USA (IN 99). The strong correlation ($r = 0.96$) between the two measurements is shown in Fig. 5b. Although the NH_3 seasonality remain consistent from 2008 to 2018 - namely spring maxima and secondary maxima in fall with lowest values in winter - both AMoN and IASI also show increasing trends of NH_3 concentrations over the entire timeseries. AMoN shows a trend of $6.5\% \cdot \text{yr}^{-1}$ while IASI shows a trend of $7.0\% \cdot \text{yr}^{-1}$.

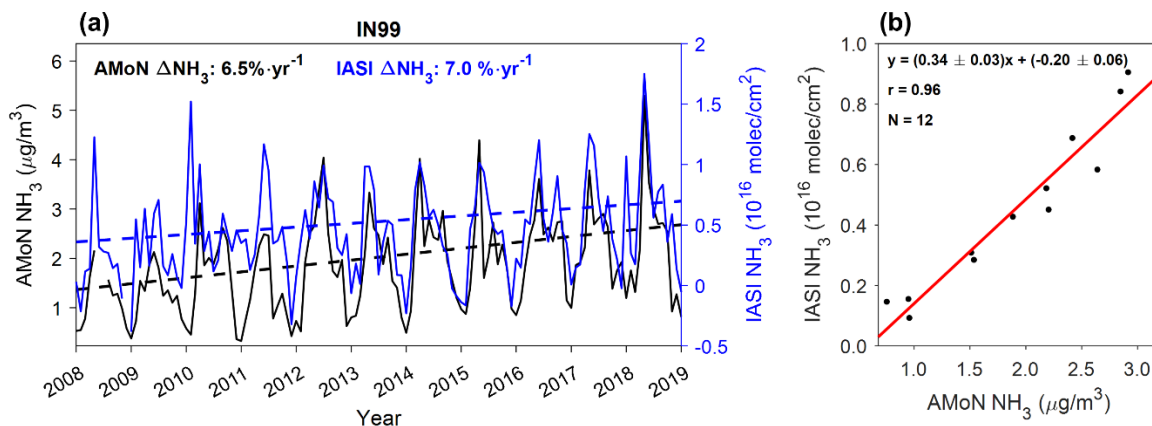


Figure 5. (a) 2008 – 2018 monthly averaged NH_3 trends for AMoN site in Indianapolis, Indiana, U.S. (IN 99) and IASI NH_3 observations within 25 km of IN 99; (b) seasonality correlation between AMoN and IASI NH_3 for IN 99.

A long-term trend analysis was performed using AMoN and IASI data to examine the agreement between the datasets and explore any regional differences. IASI NH_3 columns smaller than the 5th percentile (0.5×10^{15} molec/ cm^2) of the 11-year NH_3 average in the CONUS region were excluded to avoid spurious trend results caused by the higher noise in these measurements.

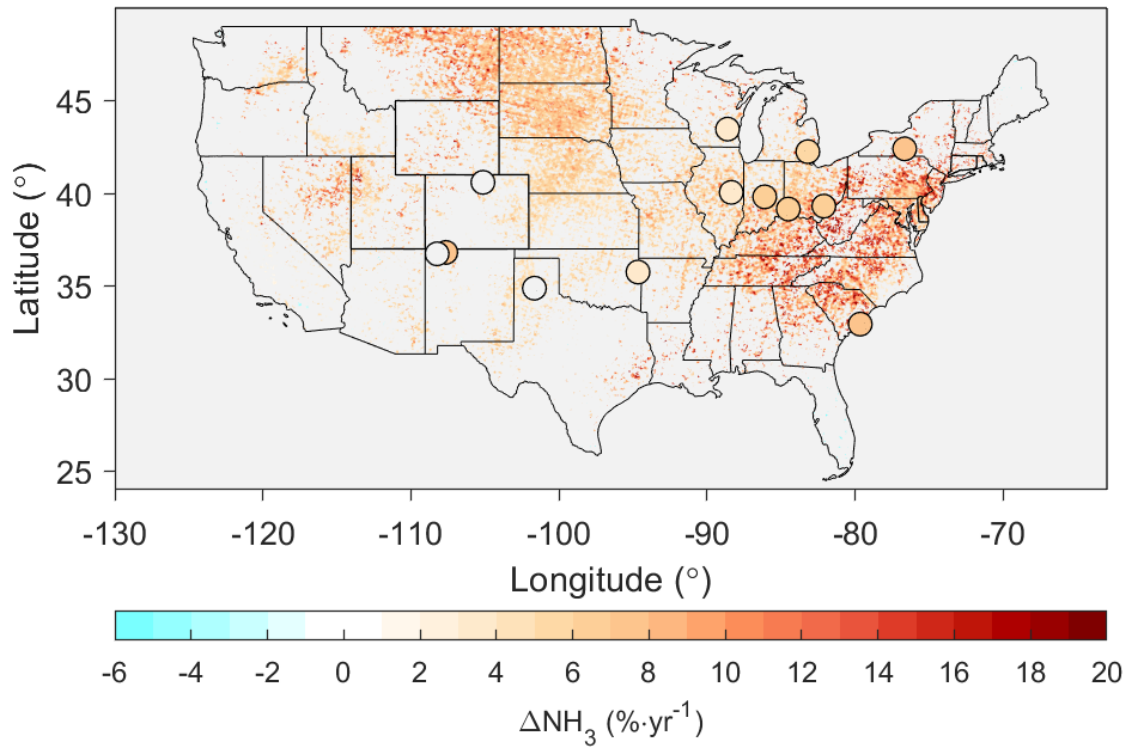
To perform the interannual trend analysis, we require each region or site to have at least one valid measurement in each season to alleviate the possible bias due to seasonal variations. Fig. 6 shows the annual percentage change for both IASI and AMoN. Most regions in the CONUS have increasing NH_3 concentrations based on the 11-year IASI observations (median: $6.8\% \cdot \text{yr}^{-1}$), including eastern U.S., Midwest, and parts of the western U.S. 10 out of 13 AMoN sites have statistically significant NH_3 increases. AMoN data in general suggest similar increases (median: $6.7\% \cdot \text{yr}^{-1}$). When plotting the trends of AMoN sites against the median of IASI trends within a 25 km spatial window (Fig. 7), a moderate correlation ($r = 0.66$) was found between IASI and AMoN NH_3 trends. IASI in general suggested a higher NH_3 increase compared to AMoN (slope: 1.26 ± 0.51) with the ratio larger than one for most sites. The absolute NH_3 change also is in correspondence with the previous study, with significant NH_3 increases across the CONUS regions, especially in the Midwest (Van Damme et al., 2021).

The spatial consistency across the datasets differs significantly. Both AMoN and IASI suggest $\sim 5\% \cdot \text{yr}^{-1}$ NH_3 increases in the Great Lake Region, while IASI suggests a higher NH_3 increase in the eastern US compared with AMoN. The IASI trend analysis results suggest a significant NH_3 increase in the northern Great Plains, e.g., North Dakota, South Dakota, and Montana, yet there are no AMoN sites in this region. Furthermore, the trends are consistent with the NH_3 emissions increases caused by increased N fertilizer usage in the northern Great Plains (Cao et al., 2020b). McHale et al. (2021) showed that wet-precipitation NH_4^+ concentrations based on NADP observations suggested the highest increases in the Great Plains, the Rocky Mountain Region, and the Great Lake Region from 2000 to 2017, which is geographically consistent with the NH_3 trends observed by



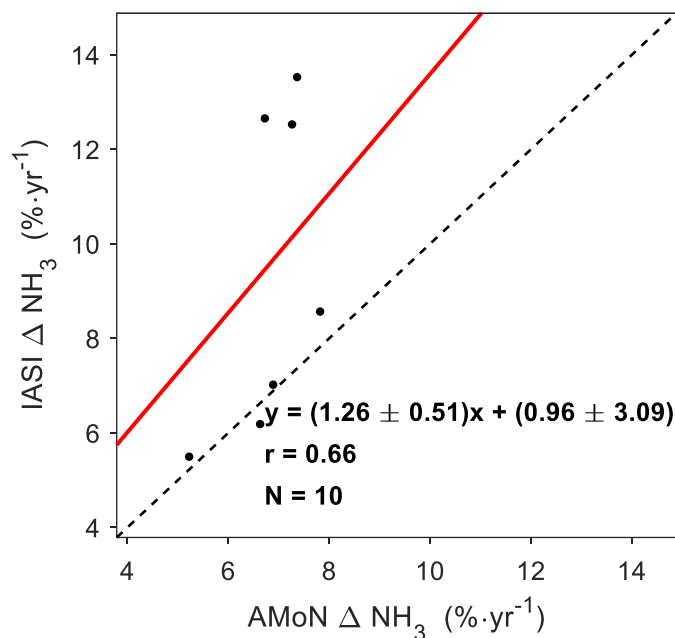
both AMoN and IASI. If considering the CONUS as a whole and calculating the annual mean NH_3 for the whole CONUS during 2008 – 2018 to derive the overall trend in CONUS, the IASI NH_3 change for 2008 – 2018 is $(3.9 \pm 2.2) \% \cdot \text{yr}^{-1}$ and $(1.3 \pm 0.8) \times 10^{14} \text{ molec/cm}^2 \cdot \text{yr}^{-1}$, similar with the trend in the previous study $(3.4 \pm 0.6) \% \cdot \text{yr}^{-1}$ and $(1.1 \pm 0.4) \times 10^{14} \text{ molec/cm}^2 \cdot \text{yr}^{-1}$ (Van Damme et al., 2021).
430

In terms of trend in NH_3 hotspots, which are here defined as regions where the IASI NH_3 column is larger than the 95th percentile of 11-year CONUS map ($6.7 \times 10^{15} \text{ molec/cm}^2$), the median of NH_3 trend is $4.7\% \cdot \text{yr}^{-1}$, indicating that the regions of the largest emissions sources are also realizing increasing concentrations over time. Although the percent changes in the regions with the highest concentrations are smaller compared with the trend in CONUS median ($8.0\% \cdot \text{yr}^{-1}$), in terms of the absolute changes, the median trend of NH_3 columns over these NH_3 hotspots are higher compared with the CONUS median ($3.7 \times 10^{14} \text{ molec/cm}^2 \cdot \text{yr}^{-1}$ vs. $2.8 \times 10^{14} \text{ molec/cm}^2 \cdot \text{yr}^{-1}$). The top 10 NH_3 hotspots in CONUS regarding column-areal weighting all exhibit increasing NH_3 concentrations from 2008 to 2018 (Table 5). Within these hotspots, the central Great Plains experience the largest NH_3 increase (median: $5.0\% \cdot \text{yr}^{-1}$, $4.0 \times 10^{14} \text{ molec/cm}^2 \cdot \text{yr}^{-1}$) while the San Joaquin Valley (median: $2.0\% \cdot \text{yr}^{-1}$, $1.6 \times 10^{14} \text{ molec/cm}^2 \cdot \text{yr}^{-1}$) and Imperial County, California (median: $2.1\% \cdot \text{yr}^{-1}$, $1.9 \times 10^{14} \text{ molec/cm}^2 \cdot \text{yr}^{-1}$) have a smaller change change.
440



445

Figure 6. Trend analysis for IASI NH₃ (2008 - 2018) and AMoN NH₃ measurements in the contiguous U.S. The gray color indicates no statistically significant change. The circle size denotes the length of AMoN data record.



450 **Figure 7.** Comparison between AMoN and IASI NH₃ trends (25 km spatial window) for AMoN sites with available nearby IASI trend data

Table 5. 2008 – 2018 IASI observed NH₃ trend in the top 10 NH₃ hotspots (column-areal weighting) in CONUS

Hotspots	% · yr ⁻¹	10 ¹⁴ molec/cm ² · yr ⁻¹
Central Great Plains	5.0	4.0
The San Joaquin Valley	2.0	1.6
North Oklahoma	3.9	2.9
Texas panhandle	3.6	2.8
Central Iowa	4.4	3.3
The Snake River Valley	3.8	3.3
Southeast Iowa	5.2	3.9



Beadle County, South Dakota	8.3	6.0
Weld County, Colorado	3.6	2.9
Imperial County, California	2.1	1.9

455 To provide a detailed insight of the increasing NH_3 over the CONUS, we further perform trend analyses for different seasons
 (Fig. 8). In spring, significant NH_3 increases are found in the Midwest and Eastern US. In summer, NH_3 increases shift to the
 western US and part of the eastern US. AMoN and IASI seasonality clustering results show that the Midwest and eastern
 United States, dominated by fertilizer NH_3 emissions, have a broad, spring maximum of NH_3 , while the western United States,
 dominated by volatilization of livestock waste NH_3 emissions, in contrast, show a narrower midsummer peak (Wang et al.,
 460 2021). The spatial patterns of spring and summer NH_3 trends are in agreement with the seasonality clustering results, indicating
 that increasing NH_3 emissions caused by agricultural activities may contribute to NH_3 concentration increase. The increasing
 wildfire activities in the western U.S. may also contribute to NH_3 increases (Lindaas et al., 2021a, b). In fall and winter, most
 regions in the U.S. do not have statistically significant IASI NH_3 trends, and a decreasing NH_3 trend is observed by IASI in
 the Southwest US in fall. In contrast, AMoN data suggest a notable NH_3 increase in Northeast and the Corn Belt region in
 465 winter. Again, IASI data are susceptible to low thermal contrasts in winter, which to some extent explains the disagreement
 between IASI and AMoN in winter as discussed in Section 3.3.

Wintertime NH_3 plays an important role in haze episodes through the formation of aerosol phase NH_4NO_3 (Shah et al., 2018;
 Zhai et al., 2021), and increasing NH_3 concentrations in winter may affect aerosol acidity and aerosol chemistry (Lawal et al.,
 470 2018; Zheng et al., 2020). In the past decades, NO_x and SO_2 emissions reductions have resulted in less NH_x partitioning into
 particle phase NH_4^+ (Shah et al., 2018), however, the partitioning alone is not able to fully explain the significant NH_3
 concentration increases (Yao and Zhang, 2019; Yu et al., 2018). The change of meteorological conditions, such as increasing
 air temperatures may also contribute to the increasing NH_3 trends (Warner et al., 2017; Yao and Zhang, 2019). No matter the
 reason for increasing NH_3 concentrations across the CONUS regions, the fact that both NH_3 surface concentrations and NH_3
 475 column concentrations are increasing during the past decade will have significant impacts on air quality and nitrogen
 deposition. EPA is reviewing the 2020 $\text{PM}_{2.5}$ National Ambient Air Quality Standard (NAAQS) currently set at $12.0 \mu\text{g}\cdot\text{m}^{-3}$
 and if the NAAQS is lowered, NH_3 controls will become increasingly important for meeting the standard. Additionally, Pan
 et al. (2021) demonstrates that NH_3 transported from Colorado significantly increased the dry NH_3 deposition the Rocky
 Mountain National Park. Increasing gas phase NH_3 may result in longer spatiotemporal scales for dry nitrogen deposition,
 480 leading to adverse impacts on remote regions and sensitive ecosystems (Phoenix, et al., 2006). Reduction of NH_3 emissions is
 critical to protect human health and the biodiversity in sensitive ecosystems (Ellis et al., 2013, Hill et al., 2019).

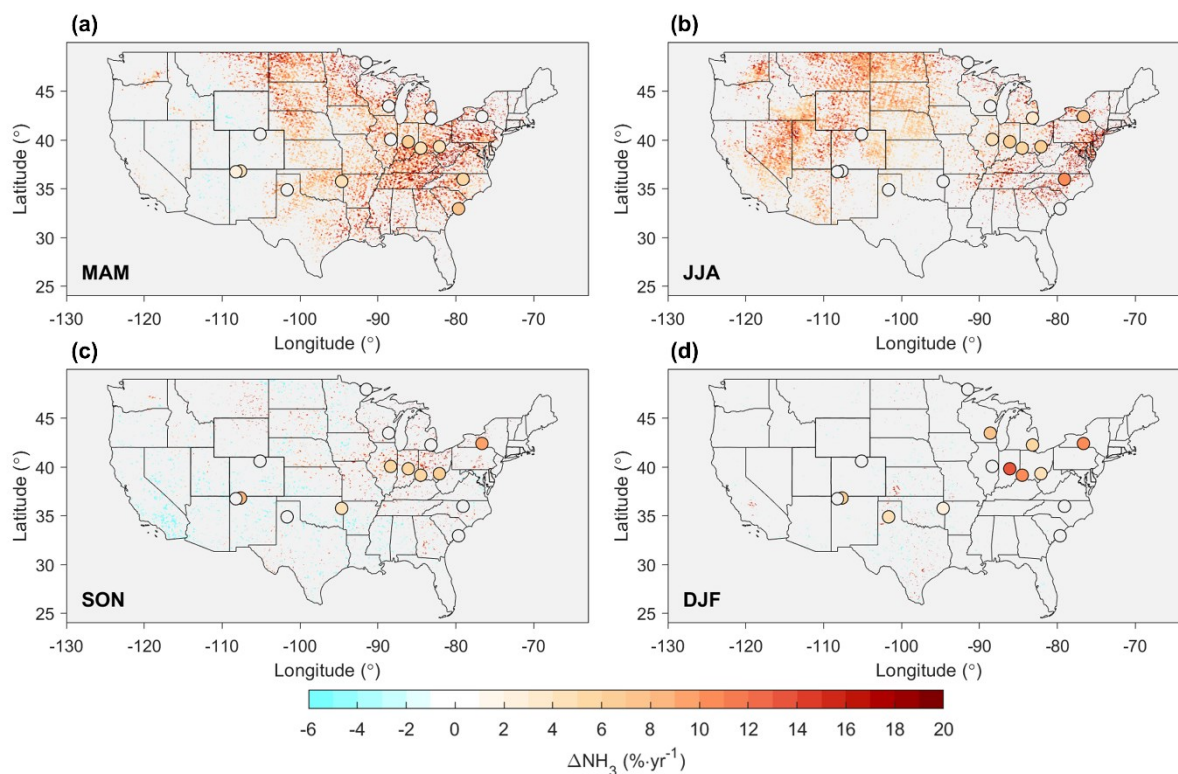


Figure 8. 2008 – 2018 NH_3 trend for different seasons based on IASI NH_3 measurements in the contiguous U.S. (a) spring (March, April, May); (b) summer (June, July, August); (c) autumn (September, October, November); (d) winter (December, January, February)

485

4.2 Trend in the urbanized areas

The short lifetime of NH_3 leads to strong spatial variabilities of NH_3 concentrations, and most AMoN sites are not located in highly populated urban regions (Wang et al., 2021). Fig. 9 shows population coverage of AMoN in the CONUS region. Population data were retrieved from the Gridded Population of the World, Version 4 (GPWv4) (Center for International Earth Science Information Network – Columbia University, 2018). More than half of the CONUS population is at least 100 km away from an AMoN site. As mentioned in the previous discussion of spatial windows, AMoN may best represent the NH_3 variations for regions within ~ 10 km radius, and less than 2% of CONUS population are within 10 km of an AMoN site. More urban AMoN sites are needed to represent the urban areas and better quantify NH_3 emissions from mobile sources, trends in the urban areas. Satellite observations are the only dataset that can currently be used to investigate source contributions and trends in population centers (Cao et al., 2022).

495

We retrieved urban area data from the 2010 US Census, which includes two different types of urban areas: Urbanized Areas (UAs) of 50,000 or more people and Urban Clusters (UCs) of at least 2,500 and less than 50,000 people (U.S. Census Bureau,



2012). The urban areas have a similar NH_3 trend compared with CONUS ($8.1\% \cdot \text{yr}^{-1}$ vs. $8.0\% \cdot \text{yr}^{-1}$), suggesting a simultaneous
 500 NH_3 increase in both urban and rural areas. The top ten most populous urbanized areas almost all exhibit significant NH_3
 increases with the exception of Miami, Florida, which has a negative trend and Dallas, Texas, without any significant trend
 (Table 6). These ten areas in total accommodate more than seventy million population, making up more than one fifth of the
 total population in the CONUS. The NH_3 increase in these densely populated areas and its impact on the aerosol chemistry
 need to be further addressed.

505

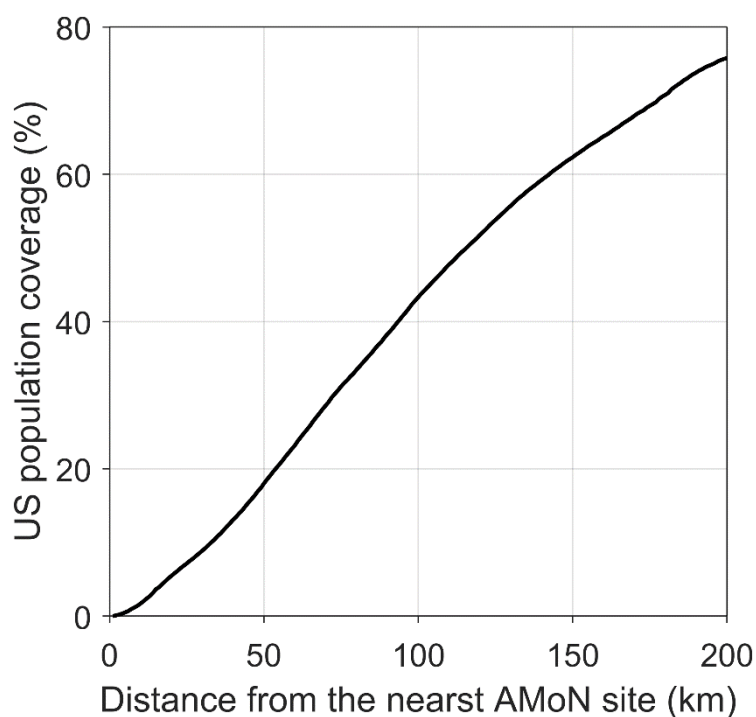


Figure 9. The population coverage of AMoN sites.

510

Table 6. 2008 – 2018 IASI NH_3 trend in the top 10 most populous urbanized areas

Urbanized Area	Population (million)	$\% \cdot \text{yr}^{-1}$	$10^{14} \text{ molec/cm}^2 \cdot \text{yr}^{-1}$
New York--Newark, NY--NJ--CT	18.0	10.8	2.0
Los Angeles--Long Beach--Anaheim, CA	12.0	4.3	2.1



Chicago, IL--IN	8.6	5.2	2.5
Miami, FL	5.5	-25.2	-1.5
Philadelphia, PA--NJ--DE--MD	5.4	10.9	2.6
Dallas--Fort Worth--Arlington, TX	5.1	/	/
Houston, TX	4.9	7.9	2.0
Washington, DC--VA--MD	4.6	9.0	2.2
Atlanta, GA	4.5	9.4	2.2
Boston, MA--NH--RI	4.2	10.5	1.4

515 **5 Implications**

Under favorable conditions, IASI NH₃ columns correlate with AMoN NH₃ surface concentrations even at the 2-week scale and for low concentration regions ($r = 0.74$ when temporal coverage $\geq 80\%$). IASI measurements' temporal coverage of AMoN's 2-week sampling period dominates the agreement presumably because of the larger day-to-day variability of NH₃. The agreement demonstrates the strong potential for using IASI NH₃ columns to bridge the spatial gaps of the AMoN network.

520 The global coverage of satellite measurements enables IASI NH₃ product to serve as an alternative dataset in countries and regions that do not have any NH₃ monitoring networks, particularly in developing countries. For example, India is the second most populated country in the world with a sixth of the world's population, and recent study has shown that the unique role of NH₃ in forming massive chloride aerosols (up to 40 $\mu\text{g}/\text{m}^3$) in India (Gunthe et al., 2021). However, there are currently no long-term NH₃ ground monitoring networks in India, impeding the efforts to estimate and control NH₃ emissions (Beale et al.,

525 2022). IASI's low sensitivity to wintertime NH₃ shows the value of the more sensitive AMoN sites. Extra attention is needed when using IASI data in such circumstances.

The increasing NH₃ in the CONUS (median: $6.8\% \cdot \text{yr}^{-1}$, $2.8 \times 10^{14} \text{ molec}/\text{cm}^2 \cdot \text{yr}^{-1}$), including the hotspots region (median: $4.7\% \cdot \text{yr}^{-1}$, $3.7 \times 10^{14} \text{ molec}/\text{cm}^2 \cdot \text{yr}^{-1}$), highlights the more important role of NH₃ in PM_{2.5} formation and nitrogen deposition

530 in the future. AMoN suggests a similar NH₃ increase ($6.7\% \cdot \text{yr}^{-1}$) as well as a similar spatial pattern with IASI. Both IASI and



AMoN show largest NH_3 increase in the Midwest and eastern U.S., with a moderate agreement for AMoN sites ($r = 0.66$). More co-located measurements of $\text{PM}_{2.5}$ mass and NH_3 concentrations would help assess the impact increasing trends of NH_3 will have on human health. The integrated satellite and ground-based measurements are already playing a role in our understanding of under-represented NH_3 emissions sources in the inventories. NH_3 already dominates the reactive nitrogen
535 deposition in the majority areas in the U.S., with the continuing efforts on NO_x emission reductions, NH_3 is expected to become the key species for nitrogen deposition (Li et al., 2016) and poses adverse impacts on the nearby ecosystem regions, e.g., the National Parks (Benedict et al., 2013; Pan et al., 2021). The changing partitioning of NH_x between NH_3 and NH_4^+ is likely to impact the lifetime of NH_x due to differences between the removal velocity of gas phase NH_3 via dry deposition and particle phase NH_4^+ wet deposition. The trends vary in different seasons, with NH_3 increases mainly in spring in the Midwest and
540 eastern U.S. (cropland dominated) while in summer in the western U.S. (feedlot dominated), suggesting the impacts from agricultural activities and the necessity of developing regionally-specific emission control strategies.

Because of the scarcity of the ground monitoring sites in the urban areas, satellite NH_3 measurements are extremely valuable to characterize NH_3 magnitude, seasonality, and trend in densely populated areas. Satellite observations suggests NH_3 increases
545 across the U.S. urban areas (median: 8.1%). New York—Newark, NY--NJ—CT alone has more than eighteen million population, experiencing an $10.8\% \cdot \text{yr}^{-1}$ NH_3 increase. Measurements from satellites will help inform where ground based NH_3 samplers could be located to better understand local air quality in overburdened communities that lack resources for continuous monitors. In addition, NH_3 sources in the urban areas and the related atmospheric chemistry are both poorly understood (Gu et al., 2022; Sun et al., 2017) and could be constrained by satellite NH_3 observations (Cao et al., 2022).
550 However, satellite observations alone are not able to answer all questions under the complex urban atmospheric conditions. For instance, gas phase NH_3 and HNO_3 can nucleate directly to form NH_4NO_3 particles in cold atmospheric conditions and is likely to result in rapid growth of new atmospheric particles in winter in urban areas (Wang et al., 2020). To provide accurate and fine spatial scale NH_3 observations in the urban areas, more routine ground monitoring sites are needed both in urban areas and high NH_3 emission source regions.

555

6 Data availability

The AMoN data were downloaded from the National Atmospheric Deposition Program/National Trends Network (NADP/NTN): <https://nadp.slh.wisc.edu/networks/ammonia-monitoring-network/>. The authors acknowledge the AERIS data infrastructure (<https://www.aeris-data.fr>) for providing access to the IASI Level 2 NH_3 data used in this study. Population data
560 were retrieved from Center for International Earth Science Information Network, Columbia University: <https://sedac.ciesin.columbia.edu/data/collection/gpw-v4/>. The urban areas data are downloaded from the U.S. Census Bureau: <https://www.census.gov/geographies/mapping-files.html>.



Author contributions

MAZ and RW designed the research; RW led the analysis; KS, DP, and XG contributed to data analysis; LC, MV, LP, and
565 CC helped with the usage of IASI data; MP helped with the usage of AMoN data; and RW wrote the paper with contributions
from all co-authors.

Competing interests

Competing interests. The contact author has declared that none of the authors has any competing interests.

Disclaimer

570 Publisher's note: Copernicus Publications remains neutral with regard to jurisdictional claims in published maps and
institutional affiliations.

Acknowledgements

Xuehui Guo gratefully acknowledges the NASA Earth and Space Science Fellowship (Grant number: 80NSSC17K0377) for
funding the work. We also gratefully acknowledge support for the analyses of the IASI and in situ data products from the
575 NASA Health and Air Quality Applied Sciences (HAQAST) team, NASA NNX16AQ90G. Mark A. Zondlo acknowledges
support as a visiting scientist at ULB from the EUMETSAT Satellite Application Facility on Atmospheric Chemistry
Monitoring (AC SAF). Kang Sun acknowledges the support from NASA Atmospheric Composition: Modeling and Analysis
Program (ACMAP, Grant number: 80NSSC19K0988). The research was funded by the Belgian State Federal Office for
Scientific, Technical and Cultural Affairs (Prodex HIRS) and the Air Liquide Foundation (TAPIR project). This work is also
580 partly supported by the FED-tWIN project ARENBERG ("Assessing the Reactive Nitrogen Budget and Emissions at Regional
and Global Scales") funded via the Belgian Science Policy Office (BELSPO). L. Clarisse is Research Associate supported by
the Belgian F.R.S.-FNRS. C. Clerbaux is grateful to CNES for scientific collaboration and financial support. The research
presented was not performed or funded by EPA and was not subject to EPA's quality system requirements. The views
expressed in this article are those of the author(s) and do not necessarily represent the views or the policies of the U.S.
585 Environmental Protection Agency.

References

Ahn, K. H. and Merwade, V.: Quantifying the relative impact of climate and human activities on streamflow, *J. Hydrol.*, 515,
257–266, <https://doi.org/10.1016/j.jhydrol.2014.04.062>, 2014.



- 590 Beale, C. A., Paulot, F., Randles, C. A., Wang, R., Guo, X., Clarisse, L., Van Damme, M., Coheur, P.-F., Clerbaux, C.,
Shephard, M. W., Dammers, E., Cady-Pereira, K., and Zondlo, M.: Large sub-regional differences of ammonia
seasonal patterns over India reveal inventory discrepancies, *Environ. Res. Lett.*, <https://doi.org/10.1088/1748-9326/AC881F>, 2022.
- Benedict, K. B., Day, D., Schwandner, F. M., Kreidenweis, S. M., Schichtel, B., Malm, W. C., and Collett, J. L.: Observations
595 of atmospheric reactive nitrogen species in Rocky Mountain National Park and across northern Colorado, *Atmos.
Environ.*, *64*, 66–76, <https://doi.org/10.1016/j.atmosenv.2012.08.066>, 2013.
- von Bobruzki, K., Braban, C. F., Famulari, D., Jones, S. K., Blackall, T., Smith, T. E. L., Blom, M., Coe, H., Gallagher, M.,
Ghalaieny, M., McGillen, M. R., Percival, C. J., Whitehead, J. D., Ellis, R., Murphy, J., Mohacsi, A., Pogany, A.,
Junninen, H., Rantanen, S., Sutton, M. A., and Nemitz, E.: Field inter-comparison of eleven atmospheric ammonia
measurement techniques, *Atmos. Meas. Tech.*, <https://doi.org/10.5194/amt-3-91-2010>, 2010.
- 600 Bouwman, A. F., Lee, D. S., Asman, W. A. H., Dentener, F. J., van der Hoek, K. W., and Olivier, J. G. J.: A global high-
resolution emission inventory for ammonia, *Global Biogeochem Cycles*, *11*, 561–587,
<https://doi.org/10.1029/97GB02266>, 1997.
- Butler, T., Vermeylen, F., Lehmann, C. M., Likens, G. E., and Puchalski, M.: Increasing ammonia concentration trends in
large regions of the USA derived from the NADP/AMoN network, *Atmos. Environ.*, *146*, 132–140,
605 <https://doi.org/10.1016/j.atmosenv.2016.06.033>, 2016.
- Cao, H., Henze, D. K., Shephard, M. W., Dammers, E., Cady-Pereira, K., Alvarado, M., Lonsdale, C., Luo, G., Yu, F., Zhu,
L., Danielson, C. G., and Edgerton, E. S.: Inverse modeling of NH₃ sources using CrIS remote sensing measurements,
Environ. Res. Lett., *15*, <https://doi.org/10.1088/1748-9326/abb5cc>, 2020a.
- Cao, H., Henze, D. K., Cady-Pereira, K., McDonald, B. C., Harkins, C., Sun, K., Bowman, K. W., Fu, T. M., and Nawaz, M.
610 O.: COVID-19 Lockdowns Afford the First Satellite-Based Confirmation That Vehicles Are an Under-recognized
Source of Urban NH₃ Pollution in Los Angeles, *Environ. Sci. Technol. Lett.*, *9*, 3–9,
https://doi.org/10.1021/ACS.ESTLETT.1C00730/ASSET/IMAGES/MEDIUM/EZ1C00730_M004.GIF, 2022.
- Cao, P., Lu, C., Zhang, J., and Khadilkar, A.: Northwestward cropland expansion and growing urea-based fertilizer use
enhanced NH₃ emission loss in the contiguous United States, *Atmos. Chem. Phys.*, *20*, 11907–11922,
615 <https://doi.org/10.5194/acp-20-11907-2020>, 2020b.
- Chen, Y., Shen, H., Kaiser, J., Hu, Y., Capps, S., Zhao, S., Hakami, A., Shih, J.-S., Pavur, G., Turner, M., Henze, D., Resler,
J., Nenes, A., Napelenok, S., Bash, J., Fahey, K., Carmichael, G., Chai, T., Clarisse, L., Coheur, P.-F., van Damme,
M., and Russell, A.: High-resolution Hybrid Inversion of IASI Ammonia Columns to Constrain U.S. Ammonia
Emissions Using the CMAQ Adjoint Model, *Atmos. Chem. Phys.*, 1–25, <https://doi.org/10.5194/acp-2020-523>, 2020.
- 620 Clarisse, L., Clerbaux, C., Dentener, F., Hurtmans, D., and Coheur, P.-F.: Global ammonia distribution derived from infrared
satellite observations, *Nat. Geosci.*, *2*, 479–483, <https://doi.org/10.1038/ngeo551>, 2009.



- Clarisse, L., Shephard, M. W., Dentener, F., Hurtmans, D., Cady-Pereira, K., Karagulian, F., van Damme, M., Clerbaux, C., and Coheur, P. F.: Satellite monitoring of ammonia: A case study of the San Joaquin Valley, *J. Geophys. Res. Atmos.*, 115, 1–15, <https://doi.org/10.1029/2009JD013291>, 2010.
- 625 Dammers, E., Palm, M., Damme, M. van, Vigouroux, C., Smale, D., Conway, S., Toon, G. C., Jones, N., Nussbaumer, E., Warneke, T., Petri, C., Clarisse, L., Clerbaux, C., Hermans, C., Lutsch, E., Strong, K., Hannigan, J. W., Nakajima, H., Morino, I., Herrera, B., Stremme, W., Grutter, M., Schaap, M., Kruit, R. J. W., Notholt, J., Coheur, P.-F., and Erismann, J. W.: An evaluation of IASI-NH 3 with ground-based Fourier transform infrared spectroscopy measurements, *Atmos. Chem. Phys.*, 16, 10351–10368, <https://doi.org/10.5194/acp-16-10351-2016>, 2016.
- 630 Dammers, E., Shephard, M. W., Palm, M., Cady-Pereira, K., Capps, S., Lutsch, E., Strong, K., Hannigan, J. W., Ortega, I., Toon, G. C., Stremme, W., Grutter, M., Jones, N., Smale, D., Siemons, J., Hrpcek, K., Tremblay, D., Schaap, M., Notholt, J., and Willem Erismann, J.: Validation of the CrIS fast physical NH₃ retrieval with ground-based FTIR, *Atmos. Meas. Tech.*, 10, 2645–2667, <https://doi.org/10.5194/amt-10-2645-2017>, 2017.
- EPA, United States Environmental Protection Agency, Air Quality Implementation Plans, <https://www.epa.gov/air-quality-implementation-plans>, last access: January 2023.
- 635 Ellis, R. A., Jacob, D. J., Sulprizio, M. P., Zhang, L., Holmes, C. D., Schichtel, B. A., Blett, T., Porter, E., Pardo, L. H., and Lynch, J. A. Present and future nitrogen deposition to national parks in the united states: Critical load exceedances. *Atmos. Chem. Phys.*, 13, 9083–9095. <https://doi.org/10.5194/ACP-13-9083-2013>, 2013
- Erismann, J. W., Sutton, M. A., Galloway, J., Klimont, Z., and Winiwarter, W.: How a century of ammonia synthesis changed the world, *Nat. Geosci.*, 1, 636–639, <https://doi.org/10.1038/ngeo325>, 2008.
- 640 Fehsenfeld, F. C., Huey, L. G., Leibrock, E., Dissly, R., Williams, E., Ryerson, T. B., Norton, R., Sueper, D. T., and Hartsell, B.: Results from an informal intercomparison of ammonia measurement techniques, *J. Geophys. Res. Atmos.*, 107, <https://doi.org/10.1029/2001JD001327>, 2002.
- Fountoukis, C. and Nenes, A.: ISORROPIAII: A computationally efficient thermodynamic equilibrium model for K⁺-Ca²⁺-Mg²⁺-NH₄⁺-Na⁺-SO₄²⁻-NO₃⁻-Cl⁻-H₂O aerosols, *Atmos. Chem. Phys.*, 7, 4639–4659, <https://doi.org/10.5194/acp-7-4639-2007>, 2007.
- 645 Goldberg, D. L., Anenberg, S. C., Lu, Z., Streets, D. G., Lamsal, L. N., McDuffie, E., and Smith, S. J.: Urban NO_x emissions around the world declined faster than anticipated between 2005 and 2019, *Environ. Res. Lett.*, 16, 115004, <https://doi.org/10.1088/1748-9326/AC2C34>, 2021.
- 650 Golston, L. M., Pan, D., Sun, K., Tao, L., Zondlo, M. A., Eilerman, S. J., Peischl, J., Neuman, J. A., and Floerchinger, C.: Variability of Ammonia and Methane Emissions from Animal Feeding Operations in Northeastern Colorado, *Environ. Sci. Technol.*, 54, 11015–11024, <https://doi.org/10.1021/acs.est.0c00301>, 2020.
- Gu, M., Pan, Y., Sun, Q., Walters, W. W., Song, L., and Fang, Y.: Is fertilization the dominant source of ammonia in the urban atmosphere, *Sci. Total Environ.*, 838, 155890, <https://doi.org/10.1016/J.SCITOTENV.2022.155890>, 2022.



- 655 Gunthe, S. S., Liu, P., Panda, U., Raj, S. S., Sharma, A., Darbyshire, E., Reyes-Villegas, E., Allan, J., Chen, Y., Wang, X., Song, S., Pöhlker, M. L., Shi, L., Wang, Y., Kommula, S. M., Liu, T., Ravikrishna, R., McFiggans, G., Mickley, L. J., Martin, S. T., Pöschl, U., Andreae, M. O., and Coe, H.: Enhanced aerosol particle growth sustained by high continental chlorine emission in India, *Nat. Geosci.*, 14, 77–84, <https://doi.org/10.1038/s41561-020-00677-x>, 2021.
- 660 Guo, X., Wang, R., Pan, D., Zondlo, M. A., Clarisse, L., van Damme, M., Whitburn, S., Coheur, P. F., Clerbaux, C., Franco, B., Golston, L. M., Wendt, L., Sun, K., Tao, L., Miller, D., Mikoviny, T., Müller, M., Wisthaler, A., Tevlin, A. G., Murphy, J. G., Nowak, J. B., Roscioli, J. R., Volkamer, R., Kille, N., Neuman, J. A., Eilerman, S. J., Crawford, J. H., Yacovitch, T. I., Barrick, J. D., and Scarino, A. J.: Validation of IASI Satellite Ammonia Observations at the Pixel Scale Using In Situ Vertical Profiles, *J. Geophys. Res. Atmos.*, 126, <https://doi.org/10.1029/2020JD033475>, 2021.
- 665 Hauglustaine, D. A., Balkanski, Y., and Schulz, M.: A global model simulation of present and future nitrate aerosols and their direct radiative forcing of climate, *Atmos. Chem. Phys.*, 14, 11031–11063, <https://doi.org/10.5194/acp-14-11031-2014>, 2014.
- Hennigan, C. J., Izumi, J., Sullivan, A. P., Weber, R. J., and Nenes, A.: A critical evaluation of proxy methods used to estimate the acidity of atmospheric particles, *Atmos. Chem. Phys.*, 15, 2775–2790, <https://doi.org/10.5194/acp-15-2775-2015>, 2015.
- 670 Hill, J., Goodkind, A., Tessum, C., Thakrar, S., Tilman, D., Polasky, S., Smith, T., Hunt, N., Mullins, K., Clark, M., and Marshall, J.: Air-quality-related health damages of maize, *Nat. Sustain.*, 2, 397–403, <https://doi.org/10.1038/s41893-019-0261-y>, 2019.
- Holt, J., Selin, N. E., and Solomon, S.: Changes in inorganic fine particulate matter sensitivities to precursors due to large-scale us emissions reductions, *Environ Sci Technol*, 49, 4834–4841, <https://doi.org/10.1021/acs.est.5b00008>, 2015.
- 675 Kendall, M.: Rank correlation methods (4th edn.) charles griffin. San Francisco, CA, 1975.
- Kharol, S. K., Shephard, M. W., McLinden, C. A., Zhang, L., Sioris, C. E., O'Brien, J. M., Vet, R., Cady-Pereira, K. E., Hare, E., Siemons, J., and Krotkov, N. A.: Dry Deposition of Reactive Nitrogen From Satellite Observations of Ammonia and Nitrogen Dioxide Over North America, *Geophys. Res. Lett.*, 45, 1157–1166, <https://doi.org/10.1002/2017GL075832>, 2018.
- 680 Lawal, A. S., Guan, X., Liu, C., Henneman, L. R. F., Vasilakos, P., Bhogineni, V., Weber, R. J., Nenes, A., and Russell, A. G.: Linked Response of Aerosol Acidity and Ammonia to SO₂ and NO_x Emissions Reductions in the United States, *Environ. Sci. Technol.*, <https://doi.org/10.1021/acs.est.8b00711>, 2018.
- Li, Y., Schichtel, B. A., Walker, J. T., Schwede, D. B., Chen, X., Lehmann, C. M. B., Puchalski, M. A., Gay, D. A., and Collett, J. L.: Increasing importance of deposition of reduced nitrogen in the United States, *Proc. Natl. Acad. Sci. U.S.A.*, 113, 5874–5879, <https://doi.org/10.1073/pnas.1525736113>, 2016.
- 685 Lindaas, J., Pollack, I. B., Garofalo, L. A., Pothier, M. A., Farmer, D. K., Kreidenweis, S. M., Campos, T. L., Flocke, F., Weinheimer, A. J., Montzka, D. D., Tyndall, G. S., Palm, B. B., Peng, Q., Thornton, J. A., Permar, W., Wielgasz, C., Hu, L., Ottmar, R. D., Restaino, J. C., Hudak, A. T., Ku, I. T., Zhou, Y., Sive, B. C., Sullivan, A., Collett, J. L., and



- 690 Fischer, E. v.: Emissions of Reactive Nitrogen From Western U.S. Wildfires During Summer 2018, *Journal of Geophysical Research: Atmospheres*, 126, <https://doi.org/10.1029/2020JD032657>, 2021a.
- Lindaas, J., Pollack, I. B., Calahorrano, J. J., O'Dell, K., Garofalo, L. A., Pothier, M. A., Farmer, D. K., Kreidenweis, S. M., Campos, T., Flocke, F., Weinheimer, A. J., Montzka, D. D., Tyndall, G. S., Apel, E. C., Hills, A. J., Hornbrook, R. S., Palm, B. B., Peng, Q., Thornton, J. A., Permar, W., Wielgasz, C., Hu, L., Pierce, J. R., Collett, J. L., Sullivan, A. P., and Fischer, E. v.: Empirical Insights Into the Fate of Ammonia in Western U.S. Wildfire Smoke Plumes, *Journal of Geophysical Research: Atmospheres*, 126, <https://doi.org/10.1029/2020JD033730>, 2021b.
- 695 Malm, W. C., Schichtel, B. A., Pitchford, M. L., Ashbaugh, L. L., and Eldred, R. A.: Spatial and monthly trends in speciated fine particle concentration in the United States, *J. Geophys. Res. Atmos.*, 109, n/a-n/a, <https://doi.org/10.1029/2003JD003739>, 2004.
- Miller, D. J., Sun, K., Tao, L., Pan, D., Zondlo, M. A., Nowak, J. B., Liu, Z., Diskin, G., Sachse, G., Beyersdorf, A., Ferrare, R., and Scarino, A. J.: Ammonia and methane dairy emission plumes in the San Joaquin valley of California from individual feedlot to regional scales, *J. Geophys. Res. Atmos.*, 120, 9718–9738, <https://doi.org/10.1002/2015JD023241>, 2015.
- 700 McHale, M. R., Ludtke, A. S., Wetherbee, G. A., Burns, D. A., Nilles, M. A., and Finkelstein, J. S.: Trends in precipitation chemistry across the U.S. 1985–2017: Quantifying the benefits from 30 years of Clean Air Act amendment regulation, *Atmos. Environ.*, 247, <https://doi.org/10.1016/J.ATMOSENV.2021.118219>, 2021.
- 705 NADP, National Atmospheric Deposition Program, the Ammonia Monitoring Network, <https://nadp.slh.wisc.edu/networks/ammonia-monitoring-network/>, last accessed: January 2023.
- Nair, A. A. and Yu, F.: Quantification of atmospheric ammonia concentrations: A review of its measurement and modeling, <https://doi.org/10.3390/atmos11101092>, 1 October 2020.
- 710 Nair, A. A., Yu, F., and Luo, G.: Spatioseasonal Variations of Atmospheric Ammonia Concentrations Over the United States: Comprehensive Model-Observation Comparison, *J. Geophys. Res. Atmos.*, 124, 6571–6582, <https://doi.org/10.1029/2018JD030057>, 2019.
- Pan, D., Mauzerall, D. L., Benedict, K. B., Wang, R., Golston, L., Collett, J. L., Jr., Tao, L., Sun, K., Guo, X., Schichtel, B. A., Ham, J. M., Prenni, A. J., Puchalski, M., Mikoviny, T., Müller, M., Wisthaler, A., and Zondlo, M. A.: A Paradigm Shift in Sulfate-Nitrate-Ammonium Aerosol Formation in the United States and its Implications for Reactive Nitrogen Deposition, *American Geophysical Union Fall Meeting 2020*, Online, 1-17 Dec. 2020, A074-06, <https://agu.confex.com/agu/fm20/meetingapp.cgi/Paper/679051>, 2020.
- 715 Pan, D., Benedict, K. B., Golston, L. M., Wang, R., Collett, J. L., Tao, L., Sun, K., Guo, X., Ham, J., Prenni, A. J., Schichtel, B. A., Mikoviny, T., Mü, M., Wisthaler, A., and Zondlo, M. A.: Ammonia Dry Deposition in an Alpine Ecosystem Traced to Agricultural Emission Hotspots, *Environ. Sci. Technol.*, 55, 7785, <https://doi.org/10.1021/acs.est.0c05749>, 2021.
- 720



- Paulot, F., Jacob, D. J., Pinder, R. W., Bash, J. O., Travis, K., and Henze, D. K.: Ammonia emissions in the United States, European Union, and China derived by high-resolution inversion of ammonium wet deposition data: Interpretation with a new agricultural emissions inventory (MASAGE_NH3), *J. Geophys. Res. Atmos.*, 119, 4343–4364, <https://doi.org/10.1002/2013JD021130>, 2014.
- 725 Phoenix, G. K., Hicks, W. K., Cinderby, S., Kuylenstierna, J. C. I., Stock, W. D., Dentener, F. J., Giller, K. E., Austin, A. T., Lefroy, R. D. B., Gimeno, B. S., Ashmore, M. R., and Ineson, P.: Atmospheric nitrogen deposition in world biodiversity hotspots: The need for a greater global perspective in assessing N deposition impacts, *Glob. Chang. Biol.*, 12, 470–476, <https://doi.org/10.1111/j.1365-2486.2006.01104.x>, 2006.
- 730 Pinder, R. W., Gilliland, A. B., and Dennis, R. L.: Environmental impact of atmospheric NH₃ emissions under present and future conditions in the eastern United States, *Geophys. Res. Lett.*, 35, 1–6, <https://doi.org/10.1029/2008GL033732>, 2008.
- Puchalski, M. A., Sather, M. E., Walker, J. T., Lehmann, C. M. B., Gay, D. A., Mathew, J., and Robarge, W. P.: Passive ammonia monitoring in the United States: Comparing three different sampling devices, *Journal of Environmental Monitoring*, 13, 3156–3167, <https://doi.org/10.1039/C1EM10553A>, 2011.
- 735 Puchalski, M. A., Rogers, C. M., Baumgardner, R., Mishoe, K. P., Price, G., Smith, M. J., Watkins, N., and Lehmann, C. M.: A statistical comparison of active and passive ammonia measurements collected at Clean Air Status and Trends Network (CASTNET) sites, *Environ. Sci.: Process. Impacts*, <https://doi.org/10.1039/c4em00531g>, 2015.
- Schiferl, L. D., Heald, C. L., Damme, M. van, Clarisse, L., Clerbaux, C., Coheur, P., Nowak, J. B., Neuman, J. A., Herndon, S. C., Roscioli, J. R., and Eilerman, S. J.: Interannual variability of ammonia concentrations over the United States: sources and implications, *Atmos. Chem. Phys.*, 12, 12305–12328, <https://doi.org/10.5194/acp-16-12305-2016>, 2016.
- 740 Shah, V., Jaeglé, L., Thornton, J. A., Lopez-Hilfiker, F. D., Lee, B. H., Schroder, J. C., Campuzano-Jost, P., Jimenez, J. L., Guo, H., Sullivan, A. P., Weber, R. J., Green, J. R., Fiddler, M. N., Bililign, S., Campos, T. L., Stell, M., Weinheimer, A. J., Montzka, D. D., and Brown, S. S.: Chemical feedbacks weaken the wintertime response of particulate sulfate and nitrate to emissions reductions over the eastern United States, *Proc. Natl. Acad. Sci. U.S.A.*, <https://doi.org/10.1073/pnas.1803295115>, 2018.
- 745 Sun, K., Cady-Pereira, K., Miller, D. J., Tao, L., Zondlo, M. A., Nowak, J. B., Neuman, J. A., Mikoviny, T., Müller, M., Wisthaler, A., Scarino, A. J., and Hostetler, C. A.: Validation of TES ammonia observations at the single pixel scale in the San Joaquin Valley during DISCOVER-AQ, *J. Geophys. Res. Atmos.*, 120, 5140–5154, <https://doi.org/10.1002/2014JD022846>, 2015.
- 750 Sun, K., Tao, L., Miller, D. J., Pan, D., Golston, L. M., Zondlo, M. A., Griffin, R. J., Wallace, H. W., Leong, Y. J., Yang, M. M., Zhang, Y., Mauzerall, D. L., and Zhu, T.: Vehicle Emissions as an Important Urban Ammonia Source in the United States and China, *Environ. Sci. Technol.*, 51, 2472–2481, <https://doi.org/10.1021/acs.est.6b02805>, 2017.
- 755 Sun, K., Zhu, L., Cady-Pereira, K., Chan Miller, C., Chance, K., Clarisse, L., Coheur, P. F., González Abad, G., Huang, G., Liu, X., van Damme, M., Yang, K., and Zondlo, M.: A physics-based approach to oversample multi-satellite,



multispecies observations to a common grid, *Atmos. Meas. Tech.*, 11, 6679–6701, <https://doi.org/10.5194/amt-11-6679-2018>, 2018.

760 Van Damme, M., Clarisse, L., Dammers, E., Liu, X., Nowak, J. B., Clerbaux, C., Flechard, C. R., Galy-Lacaux, C., Xu, W., Neuman, J. A., Tang, Y. S., Sutton, M. A., Erisman, J. W., and Coheur, P. F.: Towards validation of ammonia (NH₃) measurements from the IASI satellite, *Atmos. Meas. Tech.*, 8, 1575–1591, <https://doi.org/10.5194/amt-8-1575-2015>, 2015.

Van Damme, M., Clarisse, L., Whitburn, S., Hadji-Lazaro, J., Hurtmans, D., Clerbaux, C., and Coheur, P. F.: Industrial and agricultural ammonia point sources exposed, *Nature*, 564, 99–103, <https://doi.org/10.1038/s41586-018-0747-1>, 2018.

765 Van Damme, M., Whitburn, S., Clarisse, L., Clerbaux, C., Hurtmans, D., and Coheur, P. F.: Version 2 of the IASI NH₃ neural network retrieval algorithm: Near-real-time and reanalysed datasets, *Atmos. Meas. Tech.*, 10, 4905–4914, <https://doi.org/10.5194/amt-10-4905-2017>, 2017.

770 Van Damme, M., Clarisse, L., Franco, B., Sutton, M. A., Erisman, J. W., Wichink Kruit, R., van Zanten, M., Whitburn, S., Hadji-Lazaro, J., Hurtmans, D., Clerbaux, C., and Coheur, P. F.: Global, regional and national trends of atmospheric ammonia derived from a decadal (2008–2018) satellite record, *Environ. Res. Lett.*, <https://doi.org/10.1088/1748-9326/abd5e0>, 1 May 2021.

Walker, J. M., Philip, S., Martin, R. v., and Seinfeld, J. H.: Simulation of nitrate, sulfate, and ammonium aerosols over the United States, *Atmos. Chem. Phys.*, 12, 11213–11227, <https://doi.org/10.5194/acp-12-11213-2012>, 2012.

775 Wang, M., Kong, W., Marten, R., He, X. C., Chen, D., Pfeifer, J., Heitto, A., Kontkanen, J., Dada, L., Kürten, A., Yli-Juuti, T., Manninen, H. E., Amanatidis, S., Amorim, A., Baalbaki, R., Baccharini, A., Bell, D. M., Bertozzi, B., Bräkling, S., Brilke, S., Murillo, L. C., Chiu, R., Chu, B., de Menezes, L. P., Duplissy, J., Finkenzeller, H., Carracedo, L. G., Granzin, M., Guida, R., Hansel, A., Hofbauer, V., Krechmer, J., Lehtipalo, K., Lamkaddam, H., Lampimäki, M., Lee, C. P., Makhmutov, V., Marie, G., Mathot, S., Mauldin, R. L., Mentler, B., Müller, T., Onnela, A., Partoll, E., Petäjä, T., Philippov, M., Pospisilova, V., Ranjithkumar, A., Rissanen, M., Rörup, B., Scholz, W., Shen, J., Simon, M., Sipilä, M., Steiner, G., Stolzenburg, D., Tham, Y. J., Tomé, A., Wagner, A. C., Wang, D. S., Wang, Y., Weber, S. K.,
780 Winkler, P. M., Wlasits, P. J., Wu, Y., Xiao, M., Ye, Q., Zauner-Wieczorek, M., Zhou, X., Volkamer, R., Riipinen, I., Dommen, J., Curtius, J., Baltensperger, U., Kulmala, M., Worsnop, D. R., Kirkby, J., Seinfeld, J. H., El-Haddad, I., Flagan, R. C., and Donahue, N. M.: Rapid growth of new atmospheric particles by nitric acid and ammonia condensation, *Nature*, 581, 184–189, <https://doi.org/10.1038/s41586-020-2270-4>, 2020.

785 Wang, R., Guo, X., Pan, D., Kelly, J. T., Bash, J. O., Sun, K., Paulot, F., Clarisse, L., van Damme, M., Whitburn, S., Coheur, P. F., Clerbaux, C., and Zondlo, M. A.: Monthly Patterns of Ammonia Over the Contiguous United States at 2-km Resolution, *Geophys. Res. Lett.*, 48, <https://doi.org/10.1029/2020GL090579>, 2021.

Warner, J. X., Wei, Z., Larrabee Strow, L., Dickerson, R. R., and Nowak, J. B.: The global tropospheric ammonia distribution as seen in the 13-year AIRS measurement record, *Atmos. Chem. Phys.*, 16, 5467–5479, <https://doi.org/10.5194/acp-16-5467-2016>, 2016.



- 790 Warner, J. X., Dickerson, R. R., Wei, Z., Strow, L. L., Wang, Y., and Liang, Q.: Increased atmospheric ammonia over the world's major agricultural areas detected from space, *Geophys. Res. Lett.*, 44, 2875–2884, <https://doi.org/10.1002/2016GL072305>, 2017.
- Whitburn, S., van Damme, M., Clarisse, L., Bauduin, S., Heald, C. L., Hadji-Lazaro, J., Hurtmans, D., Zondlo, M. A., Clerbaux, C., and Coheur, P.-F.: A flexible and robust neural network IASI-NH 3 retrieval algorithm, *J. Geophys. Res. Atmos.*, 121, 6581–6599, <https://doi.org/10.1002/2016JD024828>, 2016.
- 795 Yao, X. and Zhang, L.: Trends in atmospheric ammonia at urban, rural, and remote sites across North America, *Atmos. Chem. Phys.*, 16, 11465–11475, <https://doi.org/10.5194/acp-16-11465-2016>, 2016.
- Yao, X. and Zhang, L.: Causes of Large Increases in Atmospheric Ammonia in the Last Decade across North America, *ACS Omega*, 4, 22133–22142, <https://doi.org/10.1021/acsomega.9b03284>, 2019.
- 800 Yu, F., Nair, A. A., and Luo, G.: Long-Term Trend of Gaseous Ammonia Over the United States: Modeling and Comparison With Observations, *J. Geophys. Res. Atmos.*, 123, 8315–8325, <https://doi.org/10.1029/2018JD028412>, 2018.
- Yue, S. and Wang, C. Y.: The Mann-Kendall test modified by effective sample size to detect trend in serially correlated hydrological series, *Water Resources Management*, <https://doi.org/10.1023/B:WARM.0000043140.61082.60>, 2004.
- Zhai, S., Jacob, D. J., Wang, X., Liu, Z., Wen, T., Shah, V., Li, K., Moch, J. M., Bates, K. H., Song, S., Shen, L., Zhang, Y., 805 Luo, G., Yu, F., Sun, Y., Wang, L., Qi, M., Tao, J., Gui, K., Xu, H., Zhang, Q., Zhao, T., Wang, Y., Lee, H. C., Choi, H., and Liao, H.: Control of particulate nitrate air pollution in China, *Nat. Geosci.*, 14, 389–395, <https://doi.org/10.1038/s41561-021-00726-z>, 2021.
- Zheng, G., Su, H., Wang, S., Andreae, M. O., Pöschl, U., and Cheng, Y.: Multiphase buffer theory explains contrasts in atmospheric aerosol acidity, *Science (1979)*, 369, 1374–1377, <https://doi.org/10.1126/SCIENCE.ABA3719>, 2020.